Advances in Photosynthesis and Respiration

Volume 26

Biophysical Techniques in Photosynthesis

Volume II

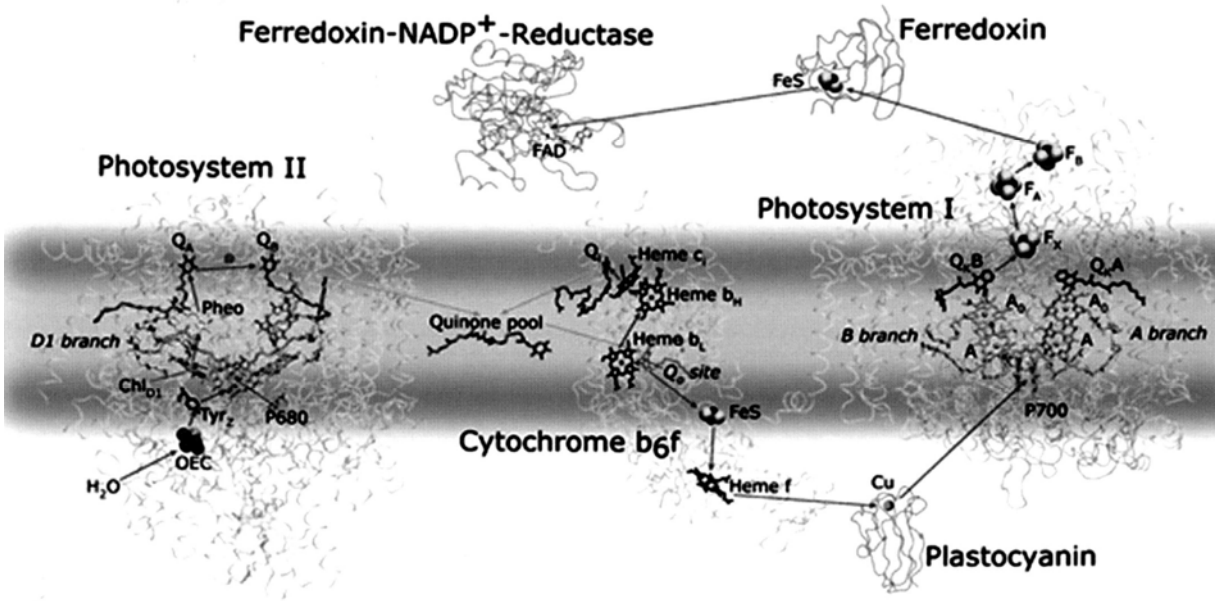

Edited by

Thijs J. Aartsma and Jörg Matysik

Springer

Chapter 9

Mass Spectrometry-Based Methods for Studying Kinetics and Dynamics in Biological Systems

Lars Konermann
Department of Chemistry, The University of Western Ontario, London, Ontario, N6A 5B7, Canada

Johannes Messinger*
Max-Planck-Institut für Bioanorganische Chemie, Stiftstraße 34 – 36, D-45470 Mülheim an der Ruhr, Germany

Warwick Hillier
Research School of Biological Sciences, The Australian National University, Canberra ACT 0200, Australia

*Author for correspondence, email: messinger@mpi-muelheim.mpg.de

Thijs J. Aartsma and Jörg Matysik (eds): Biophysical Techniques in Photosynthesis II, pp. 167–190.

Summary

In recent years, mass spectrometry (MS) has become one of the most widely used analytical techniques. MS allows studies on compounds ranging in size from single atoms to mega-Dalton biomolecular assemblies. This chapter provides an overview of recent MS applications in biophysical chemistry. The focus of our discussion is on 'time-resolved' techniques for tracking changes in complex biological reaction mixtures on time scales of milliseconds to days, thereby providing important structural and mechanistic insights. After a general introduction to biological MS, we discuss practical aspects of time-resolved membrane inlet mass spectrometry (MIMS), such as membrane properties and the use of different sample chambers. The MIMS technique allows online detection of dissolved gases and volatile compounds. It is particularly useful for resolving competing biochemical reactions involving common reactants, because isotopic labeling of substrates can be performed. As examples we present mechanistic studies on Photosystem II, carbonic anhydrase and hydrogenase. In the third part of this chapter we discuss the kinetics and mechanisms of protein folding and unfolding in solution, which can be explored via electrospray ionization mass spectrometry (ESI-MS). On-line coupling of ESI-MS with continuous-flow rapid mixing devices allows monitoring conformational changes of polypeptide chains with millisecond time resolution, as well as the detection and characterization of (un)folding intermediates. Due to its 'softness' the ESI process retains even weakly bound noncovalent complexes during the transition into the gas phase, such that protein-protein and protein-ligand interactions can be monitored directly. Additional insights into the conformational dynamics of proteins can be obtained by using time-resolved ESI-MS in conjunction with hydrogen/deuterium exchange methods. It is hoped that this chapter will stimulate the application of time-resolved MS techniques to a wide range of hitherto unexplored research areas.

I. Introduction

A. Mass Spectrometry Fundamentals

Mass spectrometry (MS) has evolved into an essential research tools for a wide range of biophysical applications. MS is capable of providing information on biological systems that is complementary to other commonly used methods such as X-ray crystallography, NMR, X-ray absorption, EPR/ENDOR, and optical or vibrational spectroscopy (Kaltashov and Eyles, 2005). Whereas spectroscopic methods generally involve the detection of electromagnetic radiation, MS measures signals induced by gas phase ions interacting with a suitable detector. To account for this fundamental difference, the term 'mass spectroscopy' should be avoided, and the correct term 'mass spectrometry' should be used instead. Nonetheless, there are analogies between the two areas. Optical spectra are plots of signal intensity vs. wavelength, whereas mass spectra display signal intensities as a function of mass-to-charge ratio (m/z). The focusing and reflection of a light beam is achieved by lenses and mirrors; an ion beam inside the vacuum chamber of a mass spectrometer can be manipulated through interactions with 'ion optics', i.e., devices employing magnetic, electric, or radio frequency fields.

Mass spectrometers encompass a few key elements, namely (*i*) ion source, (*ii*) vacuum chamber

Abbreviations: CEM – Channel electron multiplier; Da – Dalton (1 Da = 1 g/mol); DEMS – Differential electrochemical mass spectrometry; EI – electron impact (or electron ionization); ENDOR – electron nuclear double resonance; EPR – electron paramagnetic resonance; ESI – electrospray ionization; FTIR – Fourier transform infrared; HDPE – High density poly ethylene; HDX – hydrogen-deuterium exchange; MALDI – matrix-assisted laser desorption/ionization; MCP – multi channel plate; MIMS – membrane inlet mass spectrometry; MS – mass spectrometry; m/z – mass-to-charge ratio; NMR – nuclear magnetic resonance; SS – stainless steel; S/N – signal-to-noise; TOF – time-of-flight.

with pumping system, (*iii*) mass analyzer, and (*iv*) ion detector. The ion source is required to generate charged species in the gas phase from the analytes of interest. Neutral species are undetectable in MS. Ionization can be achieved by several methods, some of which will be discussed in Section I. B. Following the ionization event, the analytes are separated either in space or time within the mass analyzer. This term is somewhat misleading, because mass spectrometers separate ions according to *m/z*, not according to mass. The various types of analyzers currently being used include sector instruments (Roboz, 1968), quadrupoles and quadrupole ion traps (Douglas et al., 2005), time-of-flight (TOF) instruments (Chernushevich et al., 2001) and Fourier-transform ion cyclotron resonance mass spectrometers (Marshall et al., 1998). A discussion of the principles of these different analyzers is beyond the scope of this chapter. The requirement for vacuum is due to the fact that excessive collisions with atmospheric gas molecules would interfere with ion trajectories from the source to the detector. Elevated gas pressures would also compromise the long term stability of filaments and ion detectors.

After separation in the analyzer, the ions are detected by a suitable device. Channel electron multipliers (CEM) are the most common type of ion detector for quadrupoles and ion traps, whereas TOF instruments employ multi-channel plates (MCPs). Modern sector instruments are equipped with array detectors that allow the simultaneous monitoring of multiple analytes. The individual detection devices within these arrays can be Faraday cups (robust but with limited sensitivity) or electron multipliers (high sensitivity but less stable). In all cases, the detection principle involves the impact of ions on a metal surface which leads to the release of secondary electrons. In the case of a Faraday cup, these electrons are collected directly. CEMs and MCP detectors amplify the initial signal by several orders of magnitude before it is read out into a computer.

MS is an extraordinarily powerful tool for both quantitative and qualitative studies. The signal response from the detector (peak height or peak area) reflects the amount of material available for ionization. The linear range of detection can cover several orders of magnitude. One major advantage of MS, when compared to optical methods, is the extremely high selectivity of the technique. Optical spectra of chromophoric compounds in solution, for example, may exhibit broad absorption bands leading to spectral overlap. In contrast, the very sharp peaks observed in MS allow the detection and quantitation of multiple coexisting species in a single spectrum. The high spectral resolution of most MS techniques also permits the discrimination between various isotopically labeled forms of a single compound.

B. Ionization Techniques

Virtually any analyte, from single atoms all the way to cell organelles and intact virus particles, is amenable to mass spectrometric analysis (Heck and Van den Heuvel, 2004). The main key to a successful MS experiment is the choice of ionization method for the analyte of interest. Over the years, numerous ionization schemes have been devised, all of which ultimately result in a charged gaseous species.

One of the 'classical' approaches is referred to as electron impact (or electron ionization, EI) (Siuzdak, 1996). This method is most suitable for analyzing gases and organic compounds that readily evaporate upon heating. Exposure of gaseous analytes to an electron beam results in the formation of radical cations, schematically $M + e^- \rightarrow M^{\bullet+} + 2e^-$. In addition to intact $M^{\bullet+}$ molecular ions, EI mass spectra typically show a host of other peaks at lower *m/z* that correspond to charged fragments. The fragmentation patterns in EI-MS (also referred to as 'cracking patterns') are highly reproducible and relatively independent of the instrument used. Fingerprinting methods can therefore be employed to identify unknowns through comparison with reference spectra that are stored in computerized databases.

For several decades, MS studies were limited to relatively small compounds, ranging in size up to several hundred Daltons. The extensive fragmentation occurring with EI and other traditional ionization methods precludes studies on biological macromolecules, such as proteins and nucleic acids. A ground-breaking development was the invention of matrix-assisted laser desorption/ionization (MALDI) (Karas and Hillenkamp, 1988) and electrospray ionization (ESI) (Bruins et al., 1987; Fenn et al., 1989) in the late 1980s. The salient feature of both ionization techniques is their 'softness,' a term used to describe the fact that little or no fragmentation occurs during ion formation. Analyte charging occurs by protonation or de-protonation, thus leading to ions of the composition $[M + nH]^{n+}$ or $[M - mH]^{m-}$. Both MALDI-MS and ESI-MS are highly versatile, providing efficient means for the analysis of species

ranging from low molecular weight compounds all the way to mega-Dalton species. As a result, MS has become one of the most important analytical tools in numerous areas of chemistry, biochemistry, pharmacology, as well as for clinical research and diagnostic applications. One half of the 2002 Nobel Prize in Chemistry was awarded '*for the development of soft desorption ionisation methods for mass spectrometric analyses of biological macromolecules*' (Fenn, 2003; Tanaka, 2003).

For MALDI-MS, the analyte is embedded in a crystalline matrix that typically consists of a UV-absorbing low molecular weight compound. Exposure to a nanosecond laser pulse leads to the desorption of matrix and analyte; subsequent analyte charging occurs by proton-transfer reactions in the MALDI plume (Tanaka, 2003). For most MALDI instruments, desorption and ionization occur within the vacuum chamber of the mass spectrometer, however, the use of atmospheric pressure MALDI methods is becoming increasingly popular (Laiko et al., 2000).

ESI allows ionization to occur directly from the liquid phase. Analyte solution is infused into a metal capillary that is held at a potential of several kV. This arrangement leads to the formation of highly charged solvent droplets at the capillary tip. In case of a capillary sprayer with a positive potential, the excess charge on these droplets is primarily due to protons. Rapid solvent evaporation leads to droplet shrinkage and subsequent droplet fission, ultimately resulting in multiply protonated analyte ions in the gas phase (Kebarle and Ho, 1997). ESI occurs at atmospheric pressure. The ions generated by this process, therefore, have to be sampled and transferred into the vacuum chamber of the mass spectrometer by means of a differentially pumped interface.

C. Kinetic Studies in Solution: General Considerations

Common to kinetic studies carried out in the time domain is the use of a trigger that initiates the process of interest. The trigger event results in non-equilibrium conditions within the sample, thus giving rise to relaxation phenomena that allow the measurement of rate constants and the observation of intermediates. Optical triggers are, obviously, the method of choice for monitoring photochemical processes. Many other types of solution-phase processes can be triggered by mixing of two solutions containing the initially separated reaction partners which may be enriched isotopically above natural abundance. The use of turbulent flow or diffusion-based devices can result in mixing times as short as a few microseconds (Knight et al., 1998; Shastry et al., 1998). Manual mixing often provides sufficient temporal resolution for processes that occur on slower time scales. Kinetic experiments with MS detection may be carried out in different ways. *On-line* studies require the direct coupling of a reaction vessel to the ion source of the mass spectrometer. The composition of the reaction mixture is monitored directly, as the process of interest proceeds in solution. *Off-line* experiments usually require the availability of a quenching mechanism that stops the process of interest at well defined time points. Quenching can be achieved in various ways, e.g., by a pH-jump or by a rapid temperature change (Gross and Frey, 2002). Off-line experiments are generally more time-consuming and labor-intensive, but they allow the incorporation of sample clean-up or derivatization steps that may be required for the analysis. Due to its high sensitivity and selectivity, MS is a very attractive detection method for kinetic studies employing either on-line or off-line approaches (Houston et al., 2000; Liesener and Karst, 2005). The following sections provide examples that illustrate the wide range of possible MS applications in biophysical chemistry.

II. Time-Resolved Membrane Inlet Mass Spectrometry (TR-MIMS)

Membrane inlet mass spectrometry (MIMS) allows continuous on-line sampling of gaseous analytes (either dissolved in solution or directly from the gas phase) with a temporal resolution of a few seconds. The center piece of a MIMS experiment is a semipermeable membrane, which separates the sample matrix from the vacuum and allows gases, but not liquids to enter the mass spectrometer. MIMS obviates the need for time-consuming off-line sampling and/or gas reprocessing (e.g., the conversion of O_2 to CO_2). It is therefore ideally suited for on-line studies of photosynthesis, respiration and many other biological and technical reactions that involve gaseous reactants such as H_2, CH_4, CO, CO_2, HCN, N_2, NH_3, N_2O, NO, NO_2, O_2, H_2S, or SO_2. In addition, volatile organic molecules such as CH_3OH, C_2H_5OH, $(CH_3)_2S$ (DMS), $(CH_3)_2SO$ (DMSO) can be detected by MIMS. One particular advantage of MIMS over other techniques such as voltammetry and amperometry is that

isotopically labeled compounds can be employed to distinguish between fluxes of competing reactions; for example oxygen production ($^{16}O_2$ from $H_2{}^{16}O$) and oxygen consumption (from $^{18}O_2$) in photosynthetic algae (Radmer and Ollinger, 1980a).

A. History of TR-MIMS Instrumentation

In the early 1960s George Hoch and Bessel Kok were based in Maryland with the Martin Marietta Corporation and were studying the action spectrum of photosynthesis, when they struck upon the notion of using a mass spectrometer with a membrane to provide a liquid/vacuum interface (Hoch and Kok, 1963). This system adopted elements from the membrane approach used in 'Clark' O_2 electrodes and was developed to avoid the relatively slow equilibration processes of gas molecules at gas/liquid interfaces that are rate limiting in time resolved manometry experiments. Kok and colleagues applied the new MIMS technique to several interesting areas of research and produced many important papers in photosynthesis (Govindjee et al., 1963; Hoch et al., 1963; Radmer and Ollinger, 1980b,c, 1981, 1982, 1983, 1986). As a spin-off they also developed isotopic assays for respiration and photosynthesis, thereby providing a potential basis for discovering extraterrestrial life (Kok and Varner, 1967; Radmer and Kok, 1971; Martin et al., 1975; Radmer et al., 1976). This no doubt pleased their corporate hosts who were awarded with a prime contract from NASA to build the Viking Lander and examine life on Mars. In 1976 two Viking missions did land on Mars with mass spectrometers on board, and they did perform experiments to test for life. Ironically, however, these instruments were not MIMS systems.

B. MIMS Design Considerations

The general setup of a MIMS system is shown in Fig. 1. It consists of (*i*) a membrane-covered gas inlet system that for many applications is integrated within a sample chamber, (*ii*) a fore-line vacuum system containing two isolation valves (V_1, V_2) and a cryogenic vapor trap, and (*iii*) the mass spectrometer. In the following we discuss the function of these components and various design options.

1. Mass Spectrometer and Vacuum System

The mass analyzers used for MIMS usually employ either quadrupoles (e.g., Agilent, Waters, Thermo Electron, Shimadzu) or magnetic sector ion optics with array detection, as realized in isotope ratio mass spectrometers (e.g., GV Instruments, Thermo Electron). Quadrupole mass analyzers have several advantages; they are compact, relatively cheap, robust, easy to clean, fast scanning, require only a moderate vacuum, and are easy to adapt to varying applications. Magnetic sector field instruments with

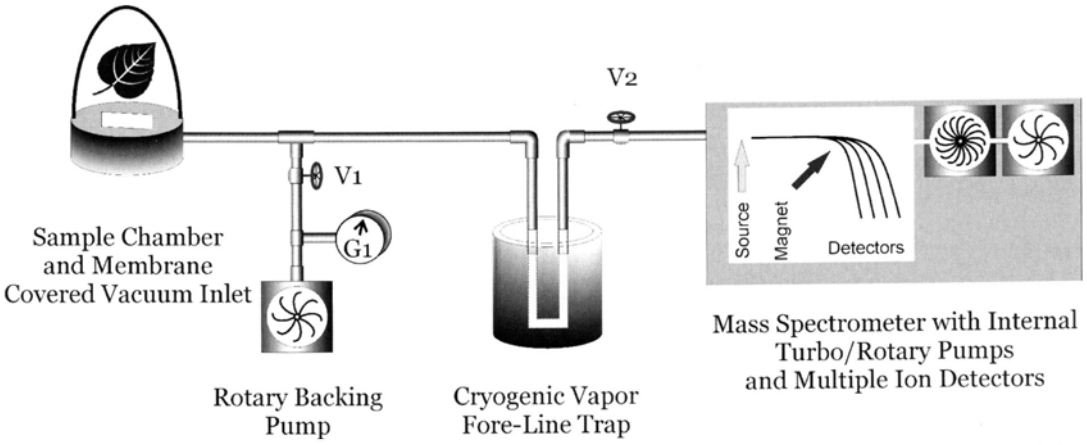

Fig. 1. An on-line MIMS system with sample chamber and membrane inlet. This system may be used with any of the cells or inlets shown in Fig. 3. A cryogenic fore-line trap removes water vapor that inadvertently penetrates through the semi-permeable membrane into the vacuum line ('fore-line') before the gases enter the mass spectrometer. The function of the isolation valves (V_1, V_2) is outlined in the text. G_1 is a vacuum gauge.

array detectors have the advantages of truly simultaneous detection of several masses and of greater sensitivity and signal stability. These points become important for isotope ratio studies. For the gaseous analytes monitored in MIMS experiments, EI is the ionization method of choice.

For the operation of MIMS systems at least two valves are required (Fig. 1). Initially valve V_2 closes the connection to the mass spectrometer. A pre-vacuum is established in the fore-line via opening valve V_1 that controls the connection to a rotary backing pump. This first step also removes water or other solvents that may still be in the cooling loop from previous measurements. Then the cryogenic vapor fore-line trap ('cryogenic trap') is engaged, by closing V_1 and slowly opening V_2. It is advisable to perform this opening with the ionization voltage switched off in order to avoid damage to the filament in case of a sudden increase in source pressure. Subsequently, data acquisition can commence.

The cryogenic trap removes trace amounts of water that inadvertently penetrate the semi-permeable membrane (see Section II.B.2). This helps to maintain an adequate vacuum within the analyzer region. The trap usually consists of a small loop in the vacuum line that runs through a Dewar containing a suitable coolant such as dry ice/ethanol (~200 K) or liquid nitrogen (77 K). One further feature of the cryogenic trap is that it safeguards against the potentially disastrous consequences of a possible membrane failure by freezing out the aqueous contents of the sample chamber before they can enter the mass spectrometer. Some care has to be taken in selecting the proper temperature and cooling loop length as to not trap the analyte(s). Condensation and boiling temperatures of some typical analytes are listed in Table 1.

For time resolved MIMS experiments the response time of the whole setup is important. Under many conditions it is the permeability of the semi-permeable membrane that is rate limiting for the signal rise (see Section II.B.2). Nevertheless, it is advisable to minimize the length of the diffusion path for the analyte by using narrow gauge stainless steel (SS) tubing (1/16–1/8´) with a total length of ≤ 60 cm to directly couple the sample chamber to the ionization chamber (Bader et al., 1983; Baltruschat, 2004). High flow turbo-molecular pumps (~200 L/s) in the mass spectrometer are also useful as high pumping rates shorten the settling time between measurements.

2. Membrane Properties

The semi-permeable membrane is the 'heart' of every MIMS set up. It is this membrane that allows the fast detection of the dissolved gases in solution by circumventing the slow transition across the liquid-gas interface. Nonetheless, its permeability often determines the response time of the whole set up, which usually is in the range of 3–10 s. The transmission of gas occurs via pervaporation. This process involves (*i*) adsorption of the analyte to the membrane surface, (*ii*) permeation through the membrane and (*iii*) desorption into the vacuum (Silva et al., 1999; Johnson et al., 2000). The gas transmission rate constant (k_{trans}) through the membrane is given by Fick's law (Hoch and Kok, 1963; Johnson et al., 2000):

$$k_{trans} = (P\,A\,\Delta p)/l \qquad (1)$$

where P is the gas permeability constant (a product of the diffusion constant D and solubility coefficient of the gas in the membrane), A is the area of the membrane inlet, Δp is the partial pressure difference across the membrane, and l is the membrane thickness. As the partial pressure of the analyte on the low pressure side of the membrane is very small, k_{trans} is proportional to the analyte concentration in the liquid phase.

The gas transmission properties of two MIMS membranes are shown in Fig. 2 as a response of the $m/z = 32$ signal to the injection of 6 nmol dissolved O_2 into the 160 µL sample chamber containing degassed water. Curve A was measured with a 25 µm thick silicone Membrane (MEM-213, Mem Pro), while trace B was obtained with a 12.5 µm thick Teflon membrane (S4, Hansatech). A range of other membranes may also be considered that might include Teflon films such as FET or AF (DuPont), silicone rubber, oxygen electrode membranes[1], or HDPE plastic films (various sources). Other possible membrane materials are listed in a recent review (Johnson et al., 2000). However, in our experience, and as shown in Fig. 2, the silicone MEM-213 membrane is one of the most permeable non-porous membrane films, resulting in fast signal rise and large signal amplitudes (see also Radmer, 1979).

The response of a MIMS system can be modeled by a series of first order rate equations. In the case of

[1] YSI provides a 12.5 µm high sensitivity and a 25.5 µm standard sensitivity Teflon membrane, Hansatech a 25 µm Teflon membrane.

Table 1: Typical mass spectral 'cracking patterns' for a number of gasses and small molecules under natural isotope enrichment (90 eV ionization energy). The peak heights are given in percent of the largest signal amplitude. (Mao and Leck, 1987).

	Hydrogen (H_2)	Helium (He)	Methane (CH_4)	Ammonia (NH_3)	Water (H_2O)	Carbon Monoxide (CO)	Nitrogen (N_2)	Nitric oxide (NO)	Methanol (CH_3OH)	Oxygen (O_2)	Hydrogen Sulfide (H_2S)	Argon (Ar)	Carbon Dioxide (CO_2)	Nitrogen Dioxide (NO_2)	Ethanol (C_2H_5OH)
Nominal mass	2	4	16	17	18	28	28	30	32	32	34	40	44	46	46
1	3		17		2										
2	100										0.2				
4		100													
12			3										10		
13			8										0.1		
14			19	2		0.8	14	8						10	
15			36	8				2							
16			100	80	2	3		2		18			16	22	
17			1	100	26										
18				0.4	100				2						6
19															2
20												23			
22													2		
26															8
27															24
28						100	100		6				13		7
29						0.7	1		65				0.1		23
30								100	0.8					100	6
31								0.4	100						100
32								0.2	67	100	44				
33									1	0.1	42				
34										0.4	100				
35											3				
36											4	0.3			
37															
38												0.1			
40												100			
42															3
43															8
44													100		
45													1		34
46													0.2	37	16
Boiling temperature (K)	20	4	112	241	373	81	77	121	338	90	212	87	195	294	352
Melting temperature (K)	14	–	91	195	273	68	63	109	176	54	152	84	216	262	159

rapid mixing (< 10 ms; see vertical sample chambers Section II.B.3.c) the injection profile is given by a step function representing the quasi-instantaneous rise in analyte concentration to c_i in the MIMS sample chamber, the overall response rate constant (k_{rise}) of the MIMS system to the change in analyte concentration, and the rate constant for the gas transfer (k_{leak}) from the sample chamber out across the membrane. The overall change in signal amplitude $I(t)$ in response to an injection at t_0 is therefore given at $t > t_0$ by:

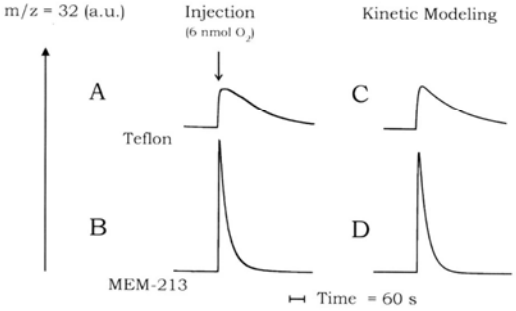

Fig. 2. Response of the $m/z = 32$ signal to the injection and rapid mixing of 6 nmol dissolved O_2 into 160 mL degassed water at 10 °C. Two different membranes were used: A, Teflon membrane (Hansatech, thickness 12.5 µm); B, MEM-213 silicone membrane (MemPro, thickness 25µm). The data can be fitted using Eq. (2), thereby providing the system response rate, k_{rise}, and the O_2 leak rate into the MS vacuum, k_{leak}. The kinetic modeling resulted in the following rate constants: C, Teflon membrane, $k_{rise} = 0.12\ s^{-1}$, $k_{leak} = 0.006\ s^{-1}$; D, Mem-213, $k_{rise} = 0.37\ s^{-1}$, $k_{leak} = 0.03\ s^{-1}$.

$$I(t) = I_0 + c_i e^{-k_{leak}(t - t_0)} K(1 - e^{-k_{rise}(t - t_0)}) \qquad (2)$$

where I_0 is the constant background signal level just before the injection, and K is a constant that accounts for the overall sensitivity of the spectrometer for a certain analyte (see also (Calvo et al., 1981). For the MIMS system used in Fig. 2, the value of k_{rise} is limited by the membrane permeability and therefore equals k_{trans} (Eq. 1) of a membrane (neglecting the effect of the boundary layer). The other kinetic term in Eq. (2) is the membrane consumption or leak rate constant (k_{leak}); this term will also depend on k_{trans} of the membrane, but is smaller because it is also inversely proportional to the sample volume, i.e. a smaller sample volume degasses faster than a larger one, if the same membrane area is used.

a. Membrane-Induced Artifacts

All factors that affect the permeability of the membrane will influence the signal intensity and stability. Outside of events leading to membrane fouling or membrane damage, the two main factors to be considered are temperature and stirring. The temperature is important because the permeability constant P in Eq. (1) is highly temperature dependent and heating will generally lead to a signal increase. Therefore, the sample chamber and membrane require efficient temperature regulation. In photochemical experiments, this may be exacerbated by the intensity and spectral properties of the actinic light, so care is needed in order to avoid heat-induced signal amplitude changes. One option to reduce light-induced artifacts is a 90° orientation between illumination and membrane.

Stirring speed is an important factor for measurements of liquid samples, because stirring critically effects the thickness of the boundary layer and thereby k_{trans} (Section II.B.3.b,c). For achieving good *S/N* ratios a constant stirring speed is essential. To this end, a good magnetic coupling between stir bar and the drive is required.

Artifacts induced by heat, light or stirring can be discovered by simultaneously monitoring the concentration of an inert internal standard such as argon, since its concentration should, in the absence of artifacts, simply decline with k_{leak}.

b. Isotope Discrimination and Calibration

When performing highly sensitive isotope-ratio measurements with a MIMS setup it is important to consider possible isotope discrimination events that might be caused by differential analyte diffusion across the membrane. Discrimination against mass (Grahams law) will occur because the thermal velocity of a gas and therefore its rate of diffusion is proportional (via D in Eq. 1) to the inverse square root of its molecular weight (see also Hoch and Kok, 1963). For the diffusion of $^{32}O_2$ and $^{34}O_2$ we obtain, for example :

$$\frac{k_{trans}(^{34}O_2)}{k_{trans}(^{32}O_2)} = \frac{\sqrt{32}}{\sqrt{34}} = 0.97 \qquad (3)$$

It should be noted that K (Eq. 2) can also be isotope dependent. Therefore, careful calibrations are required for all quantitative studies. For most gases the saturation levels for water solubility are tabulated for various temperatures and pressures (Chemical Rubber Company, 2005). Calibrations can be made by injections of known volumes of such solutions into degassed buffer in the sample chamber. For CO_2, calibration buffers can also be prepared with known concentrations of bicarbonate or carbonate at well defined pH values (enough buffer capacity is important).

c. Background Signal Determination

Background signals (especially for CO_2) can be caused for instances by sorbed gasses that leach

from the SS tubing, or by volatile molecules such as CH_3OH, C_2H_5OH, DMSO that readily penetrate the membrane and may be detected as molecular ions, or as fragmented species such as CO_2 or SO_2. Table 1 lists some possible cross contributions for some *m/z* ratios that are important for biological studies. The degree to which this is happening will depend on the abundance of the parent molecules in the sample (concentration and isotope enrichment) and the degree to which double ionization, fragmentation or gas phase reactions occur (the latter factors can be influenced by the ionization voltage). The background levels can be determined either after extensive degassing of the sample, or by selectively removing a specific gas species. O_2 can be quickly removed by a glucose, glucose oxidase, catalase oxygen scrubbing system (dithionate is not recommended because it can create a strong signal at $m/z = 32$). Solutions free of CO_2 can be obtained by preparing a dilute solution of KOH. Bubbling with argon or nitrogen within the cell are other options (Radmer and Ollinger, 1980a).

d. Membrane Support

Typical MIMS membranes are rather fragile and cannot withstand a ~1 atm pressure difference across a large inlet area without mechanical support. Ideally, this support should not produce an additional diffusion barrier. Different types of materials can be used, such as sintered glass or steel frits, porous ceramic, or porous plastic such as Teflon. In many cell designs the magnetic stirrer is in direct contact with the membrane (see Section II.B.3). This has the advantage of reducing boundary layer effects, but imposes mechanical stress.

3. Principles of Sample Chamber and Gas Inlet Design

The above criteria provide guidelines for designing MIMS systems and enable the user to tailor sample volume, membrane and inlet area for specific applications. For example, in cases where a dissolved gas is the substrate rather than the product it is best to use a sample chamber with a large volume to inlet area ratio or a membrane with low gas-permeability (Section II.B.2). Below we discuss several types of sample chamber and gas inlet designs that have been employed in laboratory and field studies. We place particular emphasis on stirring, mixing (time resolution), illumination and temperature control of these systems, but also report on capillary inlets (Section II.B.3.e) that directly probe bulk samples.

a. Unstirred Cell

The unstirred, horizontal cell is the simplest design and operates via sampling a quasi-equilibrium of the liquid phase. To improve sensitivity and increase response rate and stability experiments are usually conducted with material sedimented onto the membrane (Radmer, 1979; Radmer and Ollinger, 1982; Bader et al., 1987). The construction of such cells is typically similar to horizontally stirred cells described in detail below (Section II.B.3.b), with the exception that usually a larger inlet area is used. A variation of this design type consists of capillary inlets described in Section II.B.3.d.

b. Horizontally Stirred Cells

These cells consist of an upper sample chamber part and a lower inlet section. Both contain provisions for effective temperature control. The membrane is held and sealed at the smooth metal/metal (or plastic/metal) interface between these two components. The inner sleeve of the sample chamber is made of SS or glass and is incorporated into a brass or plastic water jacket for temperature control. Typical volumes are 1–3 mL with a ~8 mm stirrer flea (Fig. 3A). A plastic plug with a Perspex center serves as a window to the sample and closes the sample chamber to prevent atmospheric equilibration. Injections can be made via a small hole in the plug and the centre of the plug is made to accommodate an optical fiber that enables simultaneous illumination and fluorescence measurements to be performed while recording O_2 and CO_2 signals (Badger and Andrews, 1982; Hanson et al., 2003). In case of a glass inner sleeve and a transparent water jacket (commercially available for example for Clark-type electrodes from Hansatech) illumination can be made from the side. These systems can also be operated non-stirred as a gas phase chamber (Canvin et al., 1980; Maxwell et al., 1998; Ruuska et al., 2000) such as schematically depicted in Fig. 1, analogous to the Hansatech LD1/2 systems.

The inlet section (lower part) of the horizontally stirred cell is typically made out of brass or stainless steel. An insert is cut in the top for a gas-permeable membrane support and the surrounding metal surface is highly polished for a gas tight seal with the membrane (a small amount of high-vacuum grease can

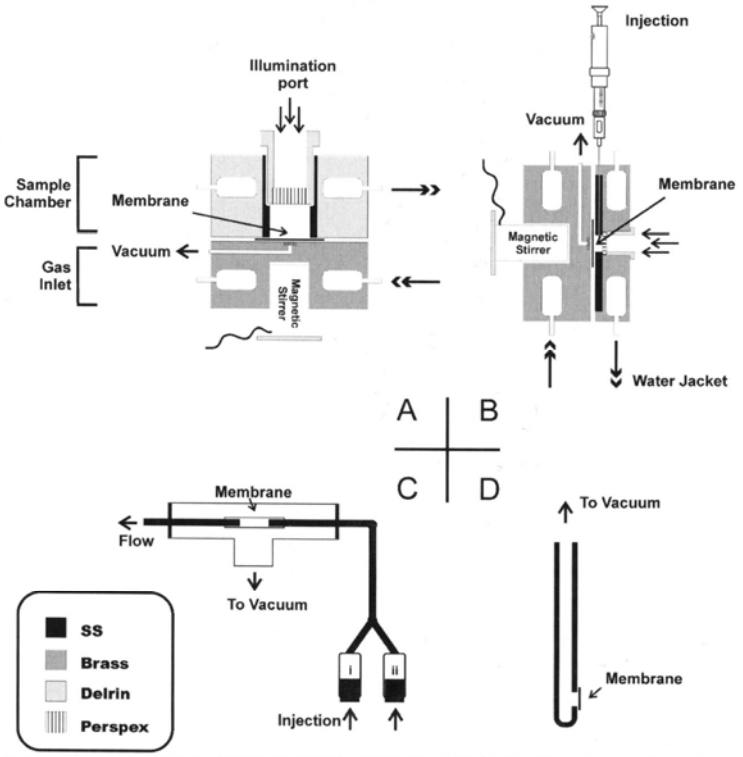

Fig. 3. Sample chambers and inlets for MIMS experiments as described in II.B.3: (A) vertically stirred cell with a removable port on the top able to accept illumination (arrows) and water jacket for temperature control (double arrows); (B) the horizontal small-volume stirred cell for the fast mixing and flash experiments; (C) a flow tube; and (D) a microprobe inlet.

be used to facilitate membrane adhesion). A vacuum line connects the cavity underneath the membrane support with the MS. This central arrangement may also contain provisions for attaching the stirrer in a defined position.

c. Vertically Stirred Cells

The vertical cell is similar to the horizontal cell but turned by 90°. This design (Messinger et al., 1995) allows experiments on photosynthetic samples with significantly reduced sample volumes (~150 µL), and it enables rapid injection/mixing experiments with isotopically labeled substrates at affordable costs. Mixing within the sample chamber is achieved via a thinned cross type stirrer bar and the rapid injection (mixing halftime ~4 ms) is made by using a modified spring loaded Hamilton (CR series) syringe that is computer triggered (Messinger et al., 1995; Hillier et al., 1998). The overall experimental time resolution of this system is in the millisecond range and is, therefore, considerably faster than that determined by k_{rise} (several seconds). This resolution is achieved via the use of a pump probe technique in which the injection of labeled substrate is followed with a variable time prior to a flash that generates the analyte (see Section II.C.1 for further details). The schematic of this sample chamber is shown in Fig. 3B. It appears feasible to achieve a similar time-resolution for non photochemical reactions by combining such a setup with a second injection that either rapidly quenches the observed reaction or releases the product.

d. Flow Tubes

Continuous flow MIMS experiments can be performed by using a set up in which the solution traverses through a SS tubing into the MS, where

the metal tubing has a gap that is bridged by a gas permeable tube or membrane (see Fig. 3C). With liquid samples, a time resolution around 2–15 s has been reported (Silverman, 1982; Johnson et al., 2000). The time resolution depends on the length of the line to the MS after the mixing point of the reactants (or of enzyme with substrate) and the flow rate (up to a few mL/min). This approach is related to the time-resolved ESI-MS experiments described in Section III.

e. Capillary Inlets

Another variation are low leak rate ('microinvasive') probes (Lloyd et al., 2002). These sampling devices operate using a semi-permeable membrane sealed to the end of a SS or quartz capillary (ID 0.1–2 mm, length up to 10 m) as inlet system. With such a probe it is possible to obtain MIMS data with spatial resolution as well as temporal resolution (Fig. 3D; Lloyd et al., 2002). By connecting such a probe to a simple quadropole, ion trap or TOF MS it is possible to assemble portable systems for the three-dimensional mapping of gases in complex ecosystems such as lakes, sediments or soils. In other applications the distribution and activity of colonies of microorganisms in food or on biofilms have been studied. A spatial resolution of less than 1 mm at a time resolution of 10–100 s (depending on membrane type and tubing length) have been reported (Lloyd et al., 2002).

4. Differential Electrochemical Mass Spectrometry (DEMS)

A very attractive experimental approach is the combination of a MIMS instrument with an electrochemical cell. This was first attempted by Bruckenstein and Gadde (Bruckenstein and Gadde, 1971), and than further developed by Wolter and Heitbaum (Wolter and Heitbaum, 1984) who also coined the name differential electrochemical mass spectrometry (DEMS). A recent overview of new technical developments in this area has been given by (Baltruschat, 2004).

A time resolution around 5 ms can be achieved by omitting cryogenic traps and by using a porous Teflon membrane. These membranes became commercially available in 1977 as Gore-Tex™ and allow the permeation of H_2O vapor while retaining liquid water. The pore size used is approximately 0.02 μm and the thickness of the membrane is 75 μm. Under these conditions the time resolution is determined by the pumping speed (differential pumping is required) and the volume of the ionization chamber (Baltruschat, 2004).

Several different cell designs have been implemented. In the simplest case the working electrode is created by painting or depositing electrode material onto the porous Teflon membrane. However, also porous rotating disc electrodes have been successfully employed as inlets (Tegtmeyer et al., 1989). Alternatively, a thin layer design with large area electrodes can be used (Hartung and Baltruschat, 1990; Baltruschat and Schmiemann, 1993). These cells are usually coupled to a quadrupole mass spectrometer.

So far the main applications of DEMS have been related to fuel cell technologies. However, in principle this technology or MIMS cells coupled with electrochemistry should also be very interesting for functional studies on redox-active proteins that produce or consume gaseous or volatile molecules.

C. Examples of MIMS Applications

Since its introduction in 1963, MIMS has revolutionized many fields with its selectivity, accuracy and its ability of continuous on-line sampling. Applications include studies on whole ecosystems and organisms, as well as mechanistic investigations on isolated enzymatic or chemical reactions. In the biophysical realm we cover three MIMS applications: photosynthetic oxygen evolution, carbonic anhydrase and hydrogenase. Other notable biophysical and biological applications include (chloro)respiration (Cournac et al., 2000), alternative oxidase (Ribas-Carbo et al., 2005), nitrogen fixation (Bader and Roben, 1995; Prior et al., 1995), denitrification (Cartaxana and Lloyd, 1999; An et al., 2001), nitric oxide (Bethke et al., 2004; Conrath et al., 2004), depth profiles of dissolved gases in oceanic waters (Tortell, 2005), and determinations of gas exchange rates of peat cores (Beckmann and Lloyd, 2001; Beckmann et al., 2004). MIMS will also be an essential tool for testing catalysts designed for artificial solar water splitting into H_2 and O_2 (Poulsen et al., 2005). Outside of the biological realm there are other fields where online MIMS sampling has made major contributions including soil, water and air analysis, fermentation and chemical reactors. Many of these more technical and environmental applications have recently been reviewed (Johnson et al., 2000) and will not be further discussed here.

1. Photosystem II Water Oxidation Chemistry

Photosystem II is a multisubunit protein complex that catalyses the light-driven oxidation of water to molecular oxygen. The reaction proceeds after four charge separation events have accumulated four oxidizing equivalents in the catalytic oxygen evolving complex (OEC) (Renger, 2001; Britt et al., 2004; McEvoy and Brudvig, 2004; Messinger, 2004; Hillier and Messinger, 2005; Yano et al., 2006). The most direct and unambiguous evidence for substrate water binding to the OEC is obtained using MIMS experiments of ^{18}O-water exchange. The measurements involve the preflashing of the sample into the desired redox state (S state) with zero to three single turn-over flashes in normal buffer media, then a small amount of $H_2{}^{18}O$ is injected and rapidly ($t_{½}$ = 4 ms) mixed. This is followed by another group of one to four closely spaced (10 ms) detecting flashes which induce oxygen evolution. The kinetics of substrate water exchange and thereby properties of the substrate water binding sites can be probed by recording the amount of labeled oxygen (*m/z* = 34 and 36) as a function of the delay between injection and the detecting flash sequence. The millisecond time resolution in these experiments therefore results from the fast mixing and signal induction (by flashes) and is not compromised by the relatively slow (seconds) detection, because the rapid photochemical production of oxygen is followed by a long dark time (10–20 s) in which no further product can be formed. The first experiments of this type were preformed using an open, unstirred sample cell (Section II.B.3.a). This resulted in a relatively long (>30 s) stabilization time between the ^{18}O-water injection and the actual photochemically measured O_2 (Radmer and Ollinger, 1980c, 1986; Bader et al., 1993). Later, a closed chamber system was developed that enabled the actual ^{18}O ligand exchange reaction of the water to be resolved (Messinger et al., 1995) (Fig. 4). In this system a stirred chamber (Section II.B.3.b; Fig. 3B) was used in conjunction with an injection system capable of equilibrating the ^{18}O-water throughout the sample chamber with $t_{½}$ ~4 ms. The use of an O_2 scavenging system (glucose/glucose oxidase/catalase) ensured that the 10–25 µL injection of ^{18}O-water was made under anaerobic conditions. This work led to the conclusion that the two substrate water molecules are bound in the OEC at two different sites (Messinger et al., 1995; Hillier et al., 1998). This discovery has

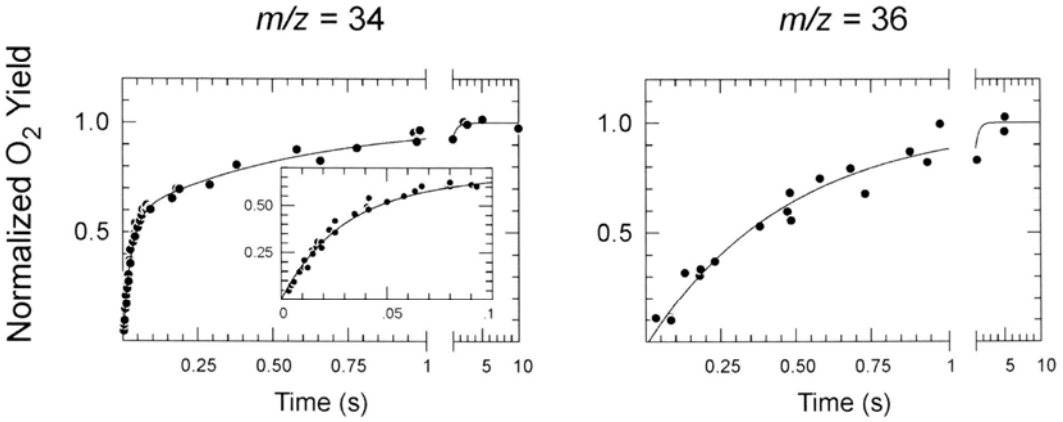

Fig. 4. MIMS-based determination of substrate water exchange rates in the S_3 state of Photosystem II in spinach thylakoids. The S_3 state is produced by two preflashes. This is followed by the injection and rapid mixing of a small amount of $H_2{}^{18}O$ (final enrichment 12%). O_2 is then produced by giving a third, detection flash at varying delay times (0–10 sec) after the $H_2{}^{18}O$ injection. Measurements were made at *m/z* = 34 (left) for the mixed labeled $^{16,18}O_2$ and at *m/z* = 36 (right) for the double labeled $^{18,18}O_2$ at 10°C. Solid lines show first-order kinetic fits yielding rate constants of 38 ± 2 s^{-1} for the fast phase (left panel) and 1.8 ± 0.2 s^{-1} for the slow phase (left and right panel). At *m/z* = 36 only the slow phase is observed, because both substrate molecules need to exchange for this signal to appear and therefore its rise is kinetically limited by the exchange at the slow exchanging substrate water binding site. This also proves that the two kinetic phases at *m/z* = 34 are not due to sample heterogeneity. All O_2 signals are normalized to the respective values obtained after complete exchange. (Hillier et al. ,1998; Hillier and Messinger, 2005, with permission).

led to further experiments that have been summarized elsewhere (Hillier and Wydrzynski, 2004; Hillier and Messinger, 2005).

MIMS has also been used to investigate other aspects of the water oxidation chemistry in Photosystem II. This includes the reactivity of the catalytic site to small reductants (NH_2OH, NH_2NH_2) that are chemically oxidized to liberate N_2 (Radmer, 1979; Radmer and Ollinger, 1982; Kretschmann and Witt, 1993) and were extended to generate a steric profile of the substrate entry site with the use of organic derivatives of hydrazine or hydroxylamine of different size (Radmer and Ollinger, 1983). One MIMS experiment has also probed the chemical oxidation of H_2O_2 to O_2 (Mano et al., 1987) using ^{18}O-labeled substrate, and others have been performed with ^{18}O-bicarbonate to examine the intrinsic rates of carbonic anhydrase activity in Photosystem II and to show that bicarbonate is not a significant substrate of the OEC (Radmer and Ollinger, 1980c; Clausen et al., 2005; Hillier et al., 2006).

2. Carbonic Anhydrase

Carbonic anhydrase (CA) catalyzes the equilibration of dissolved CO_2 with bicarbonate via the carbonic acid intermediate, according to Eq. (4) (Lindskog and Coleman, 1973).

$$HCO_3^- + H^+ \leftrightarrow H_2CO_3 \underset{k_2}{\overset{k_1}{\rightleftharpoons}} CO_2 + H_2O \quad (4)$$

This reaction plays an extremely important role for the metabolism of both plant and animal organisms (Badger and Price, 1994; Christianson and Fierke, 1996), because it facilitates the rapid chemical equilibration of dissolved CO_2 and bicarbonate in living cells, a process that is the cornerstone of much of the biology associated with respiration and photosynthetic carbon fixation.

The application of MIMS to study the CA enzymology was introduced by Silverman and colleagues in the early 1970s (Silverman and Tu, 1976; Silverman, 1982) using a flow tube approach (Section III.B.3.d; Fig. 3C). This technique analyses the activity of CA by monitoring the relatively slow isotopic equilibration between bicarbonate and CO_2 in solution that follows the much more rapid chemical equilibration. This is done by adding a known amount of $HC^{18}O_3^-$ and following the time dependent speciation of the CO_2 signals. Directly after the addition of labeled bicarbonate the $m/z = 48$ signal represents the amount of $C^{18}O^{18}O$ formed by the rapid chemical equilibration between CO_2 and bicarbonate. Then as the CA catalyzed isotopic equilibration proceeds, the $m/z = 48$ signal decays forming first the $m/z = 46$ ($C^{18}O^{16}O$) species and ultimately all ^{18}O label is diluted into the large excess of water and the $m/z = 44$ ($C^{16}O^{16}O$) species dominates. With this technique Silverman and colleagues continue to unravel the enzymatic properties of CA enzymes (Duda et al., 2005; Fisher et al., 2005), while others use this approach for elucidating mechanisms of CO_2 concentration in cyanobacteria and algae (Badger and Price, 1989; Badger et al., 1994; So et al., 1998). MIMS is one of the few techniques capable of measuring CA activity under conditions of chemical equilibrium.

3. Hydrogenase

Hydrogenases are found in many organisms, including photosynthetic ones like *Chlamydomonas reinhardtii* and *Synechocystis* PCC 6803. In presence of suitable electron donors or acceptors, hydrogenases catalyze the interconversion of H_2 into 2 H^+ and 2 e^-. Three different types exist: FeFe, NiFe and 'Fe-free' hydrogenases (the latter were recently shown to also contain one Fe) (Shima et al., 2005). In light of a possible future H_2 economy such organisms are prime targets for studying photochemical H_2-production. In absence of exogenous electron carriers H/D exchange between D_2 and H_2O can be observed that is characteristic for the activity of the catalytic centre alone, while H_2 production/consumption rates may also depend on the properties of the product and substrate channels and the electron transfer chain, which consists of FeS clusters. Both types of reactions can be conveniently followed by MIMS by recording the $m/z = 2$, 3 and 4 signals. Since most hydrogenases are O_2 sensitive it is useful to also monitor the concentration of this gas (for details see Krasna, 1978; Vignais, 2005). These types of assays allow a comparison of the activity of hydrogenases from various organisms under different conditions, and to study the mechanism of activation/deactivation in response to inhibitors such as O_2, acetylene or CO. The assay can either be performed with whole microorganisms or with highly purified protein complexes. Together with mutagenesis and crystallography, MIMS forms an essential tool for structure-function analyses in hydrogenases. In principle, one should also be able to use MIMS for studying the unusual inorganic ligands

of the catalytic sites of hydrogenases, which depending on sample condition and species may include CO, CN^-, SO, S^{2-}, O^{2-}, OH^- or O_2. Using gas chromatography, the release of a small amount of H_2S during the activation with H_2 was reported for hydrogenase isolated from *Desulfovibrio vulgaris Miyazaki F* and by pyrolysis-MS and TOF-secondary ion MS small amounts of SO and SO_2 were only released from active hydrogenases, leading to the proposal that SO is a ligand to the active site (Higuchi and Yagi, 1999; Higuchi et al., 2000).

III. Time-Resolved Electrospray Mass Spectrometry

The ESI process provides a direct bridge between solution-phase chemistry and analyte detection in the gas-phase by MS. Thus, ESI-MS has enormous potential for on-line kinetic studies (Konermann and Douglas, 2002). Following the initiation of a process by mixing of two or more reactants, solution-phase kinetics can be monitored by direct injection of the reaction mixture into the ESI source, such that the relative concentrations of multiple reactive species can be recorded as a function of time. Application of this type of experiment include mechanistic studies on bio-organic processes (Meyer et al., 2003), and enzymatic reactions (Zechel et al., 1998; Norris et al., 2001; Li et al., 2003; Wilson and Konermann, 2004).

One possible method for carrying out time-resolved ESI-MS experiments is to interface a stopped-flow device to the ESI source of the mass spectrometer (Northrop and Simpson, 1997; Kolakowski and Konermann, 2001). However, a more common approach is to carry out time-resolved ESI-MS studies in continuous-flow mode. Fig. 5 shows one possible implementation of an ESI-MS-coupled continuous-flow setup (Wilson and Konermann, 2003). This system represents a concentric capillary mixer with adjustable reaction chamber volume. In contrast to previously described continuous-flow devices (Shastry et al., 1998), the setup operates under laminar flow conditions, a fact that has to be taken into account for data analysis (Konermann, 1999; Wilson and Konermann, 2003). Reactant solutions are continuously expelled from two syringes. Syringe A is connected to the inner capillary, whereas the solution delivered by syringe B flows through the outer capillary. Mixing occurs at the end of the inner capillary. The reaction proceeds while the mixture flows towards the outlet of the apparatus, where ESI takes place. The reaction time is determined by the solution flow rate, the diameter of the outer tube, and by the distance between the mixing point and the outlet. The latter can be adjusted continuously. Kinetic experiments are performed by initially positioning the mixer directly at the ESI source. The mass spectrometer monitors the ions emitted from the sprayer, while the assembly — consisting of syringe A, inner capillary, and mixer — is slowly pulled back. These experiments provide data in three dimensions; the time axis is determined by the mixer position, the

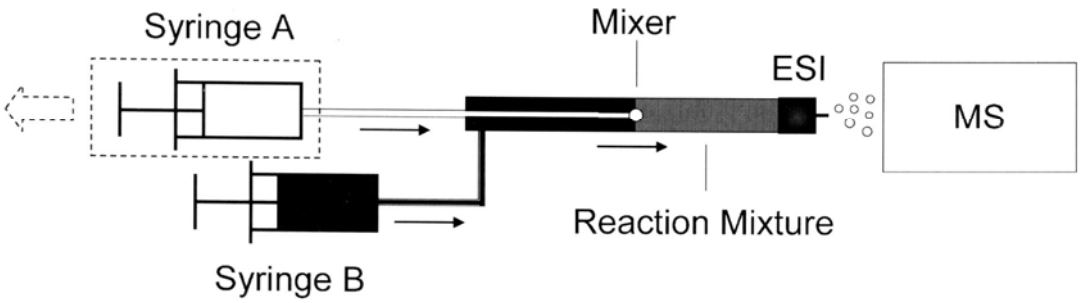

Fig. 5. Schematic depiction of a concentric capillary mixer with adjustable reaction chamber volume for time-resolved ESI-MS. Reactants are continuously expelled from syringes A and B. Mixing of the solutions from the two syringes at the outlet of the inner capillary initiates the process of interest. The reaction time can be controlled by adjusting the distance between mixer and outlet of the ESI source. This distance can be altered during the experiment by pulling back syringe A along with the inner capillary and the mixer, as indicated by the dashed block arrow. As a result, ESI-MS data can be recorded for a wide range of reaction times. Thin arrows indicate the direction of liquid flow.

m/z axis provides information on the identity of the species in the reaction mixture, and the intensity axis is related to the concentration of each of the various solution-phase species. The kinetic data obtained in this way can be visualized by either displaying mass spectra for specific reaction times, or by plotting intensity-time profiles for selected ionic species. In principle, it would also be possible to control the time axis of the experiment by altering the solution flow rate. However, this approach is not advisable because it may result in artifactual changes of analyte ion abundances (Konermann et al., 2001). One limitation of on-line ESI-MS studies is that solvent additives such as salts, buffers, and detergents which may be present in the reaction mixture can interfere with the ionization process. The use of electrosonic sprayers, fused droplet ESI, or ultra-rapid sample clean-up procedures provides possible ways to overcome this problem (Wilson and Konermann, 2005).

Global analysis methods are a powerful tool for dissecting kinetic data obtained by time-resolved ESI-MS. For chemical processes obeying first-order kinetics a master equation of the general form (Berberan-Santos and Martinho, 1990)

$$\frac{d\vec{x}}{dt} = \langle A \rangle \vec{x} \tag{5}$$

can be established, where $\vec{x} = x_1(t), \ldots, x_n(t)$ is a vector containing all time-dependent concentrations of the n species that are involved in the reaction. $\langle A \rangle$ is the $n \times n$ rate constant matrix of the system with eigenvalues $\lambda_1, \ldots \lambda_n$. Except for λ_n (which is zero), the apparent rate constants λ_j are functions of all the microscopic rate constants in the matrix. Equation (5) can be solved for any set of initial conditions, resulting in multi-exponential expressions for the concentration profiles $x_j(t)$. Accordingly, any intensity profiles, $I_i(m/z, t)$, accompanying the kinetics can be expressed as

$$I_i(m/z, t) = \sum_{j=1}^{n-1} C_{ij}(m/z) \exp(-t/\tau_j) + C_{in}(m/z) \tag{6}$$

The $(n\text{-}1)$ relaxation times, τ_j, in Eq. (6) are given by $\tau_j = (\lambda_j)^{-1}$. These τ_j values are common to all the intensity profiles $I_i(m/z, t)$, and the kinetics observed across the m/z range differ only in the amplitudes $C_{ij}(m/z)$, ..., $C_{in}(m/z)$ (Beechem et al., 1985; Holzwarth, 1995). The time resolution of the system depicted in Fig. 5 allows the measurement of relaxation times in the range of ca. 1 min down to less than 10 ms (Wilson and Konermann, 2003).

The following sections illustrate some applications of time-resolved ESI-MS for studying the folding and conformational dynamics of proteins. Space limitations preclude a discussion of kinetic studies on enzyme mechanisms, which represent another fascinating area of research (Zechel et al., 1998; Norris et al., 2001; Li et al., 2003; Wilson and Konermann, 2004). The specific examples chosen here are for water-soluble model proteins from animal organisms. It is an interesting question in how far the methodologies described here will be applicable to membrane proteins, such as those involved in photosynthetic light reactions. Initial attempts in this direction appear to be very encouraging (Whitelegge et al., 1999; Demmers et al., 2000).

A. Protein Folding and Unfolding

The three-dimensional structure adopted by the polypeptide chain of a protein depends on its solvent environment. Under physiological conditions of pH and temperature, and in the absence of chemical denaturants, most proteins fold into a unique, highly ordered, and compact structure. This 'native' conformation represents the biologically active state of a protein. Denaturing agents such as acid or heat can induce a transition to a largely disordered conformation. Many unfolded proteins spontaneously refold to their native structures once the denaturant is removed. This remarkable observation implies that all of the information required to attain the native structure is contained within the amino acid sequence of the polypeptide chain. The native state of a protein corresponds to the conformation with the lowest overall free energy, taking into account the contributions from the polypeptide chain and the surrounding solvent (Anfinsen, 1973). Although a lot of progress has been made in protein folding research over the last forty years, the question of how and why proteins fold remains one of the major unsolved problems in biophysical chemistry (Pain, 2000). The 'protein folding problem' is not only a fascinating challenge from an intellectual point of view, it also has important biomedical implications. For example, misfolding and aggregation are related to diseases like Alzheimer's, Parkinson's, Creutzfeldt-Jakob syndrome, type II diabetes, BSE ('mad cow

disease'), and many others (Dobson, 2003).

Of particular importance for the mechanistic understanding of folding and unfolding is the detection and structural characterization of transient intermediates. This task is not straightforward, mostly because the lifetimes of these species are often very short, spanning a range from microseconds to seconds, which prevents the use of X-ray or NMR methods for direct structural studies (Bachmann and Kiefhaber, 2001). Another important aspect that has received surprisingly little attention is the fact that many proteins adopt their biologically active conformation only after binding metal ions, prosthetic groups, or other proteins. Very little is known about the interplay of folding and binding, and the interactions of noncovalent binding partners with short-lived folding intermediates. Only very recently have these important questions come to the forefront of research (Shoemaker et al., 2000; Wittung-Stafshede, 2002). Time-resolved ESI-MS has the potential to address these and other questions, thus contributing to a better understanding of protein folding and unfolding in general.

As discussed in Section I.B, positive ion ESI produces intact, multiply protonated ions directly from proteins in solution. The charge states (protonation states) observed in ESI-MS are strongly dependent on the protein structure in solution. Unfolded proteins exhibit wide distributions of highly protonated ions. In contrast, tightly folded, compact structures give rise to much lower charge states and narrow distributions. While the physical reasons underlying this empirical relationship are still a matter of debate, ESI charge state distributions have become a widely used probe for the overall compactness of protein solution-phase conformations (Chowdhury et al., 1990; Konermann et al., 1997; Kaltashov and Eyles, 2002a).

Figure 6 illustrates how time-resolved ESI-MS can provide 'snapshots' of a protein folding reaction for selected time points. Ubiquitin, a small (8.6 kDa) protein, is a common model system for folding studies. Its compact native structure breaks down in acidic solutions containing organic cosolvents such as methanol, to form an extended A state that possesses an extensive non-native α-helicity (Brutscher et al., 1997). For the data depicted in Fig. 6, the transition from the denatured state back to the native protein was triggered by mixing protein solution containing a high concentration of methanol and acetic acid with excess water. The initial spectrum, recorded for t = 20 ms (Fig. 6A), shows a relatively broad charge state distribution, with the 12+ peak having the highest intensity. As refolding proceeds, the relative abundance of highly charged protein ions decreases, and that of the 8+ and 7+ ions increases (Figs. 6B, C). Refolding of ubiquitin under these conditions appears to be a simple two-state process that does not involve any kinetic intermediates.

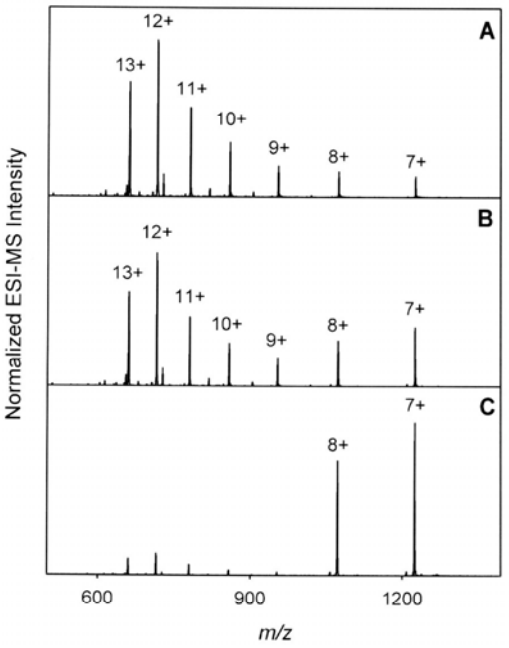

Fig. 6. Time-resolved ESI mass spectra recorded during refolding of ubiquitin. The protein was initially denatured by exposing it to 50% methanol and 4% acetic acid. Refolding was triggered by a mixing with water, resulting in a drop of the methanol and acid content to of 16% and 1.6%, respectively. Spectra were recorded 20 ms (A), 160 ms (B), and 2.1 s (C) after mixing. Notation: 'n^+' represents intact gas-phase protein ions of the composition [ubiquitin + nH]n^+. (Wilson and Konermann, 2003, with permission).

B. Assembly and Disassembly of Protein Complexes

Due to its very gentle nature, ESI allows not only the ionization of intact biopolymers, but also of multicomponent complexes that are held together by weak noncovalent interactions. Thus, assemblies involving proteins and metal ions, prosthetic groups, inhibitors, substrates, nucleic acids, and other types of ligands are amenable to ESI-MS (Heck and Van den Heuvel, 2004; Schermann et al., 2005). The ubiquitin example discussed in the previous paragraph illustrates a fold-

ing transition that does not involve any intermolecular interactions. However, structural changes of many other proteins are closely intertwined with the binding or loss of ligands. Time-resolved ESI-MS can simultaneously provide data on protein conformation and ligand binding state as a function of time.

Mammalian hemoglobins possess a heterotetrameric structure, comprising two pairs of heme-containing α and β subunits in a tetrahedral arrangement. Comparatively little effort has been directed towards the processes by which hemoglobin is formed from (or broken down into) its monomeric constituents. This is partially due to the structural heterogeneity of the protein, which makes studies on association/dissociation processes by conventional spectroscopic methods challenging. Hemoglobin exists in equilibrium between several quaternary structures, notably as monomeric (α, β), dimeric (αβ), and tetrameric ($\alpha_2\beta_2$) species. Adding to this complexity is the fact that, in principle, each of the subunits can exist in the heme-bound holo-globin form or as apo-globin (Griffith and Kaltashov, 2003).

The native state binding equilibria of hemoglobin are reflected by the presence of tetramers, dimers, and

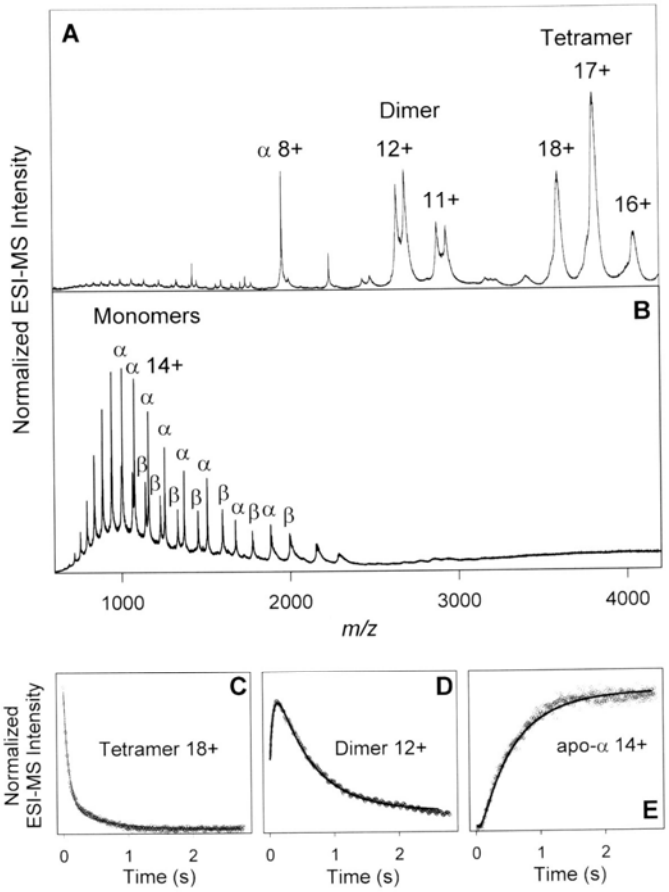

Fig. 7. (A) ESI mass spectrum of hemoglobin recorded under native solvent conditions (pH 6.8). The native tetramer appears in charge states 16+–18+. Heterodimeric species in charge states 11+ and 12+ appear as doublets due to partial loss of heme from the β subunit. (B) ESI mass spectrum of acid-denatured hemoglobin at pH 2.8. Both α and β subunits appear exclusively in their apo-forms. Panels C-E display intensity-time profiles for selected ionic species. Solid lines are the results of a global analysis procedure based on Eq. (6). (Simmons et al., 2004, with permission).

monomers in the ESI mass spectrum of Fig. 7A. Markedly different data are obtained after acid exposure of the protein, resulting in a spectrum dominated by highly charged ions that correspond to monomeric apo-α and apo-β subunits in highly unfolded conformations (Fig. 7B). These data reveal that denaturation of hemoglobin under acidic conditions results in the breakdown of the protein's quaternary structure, along with unfolding of the individual subunits and loss of heme. A detailed view of this process is obtained by using time-resolved ESI-MS for recording intensity-time profiles of all the ionic species in the spectrum (Simmons et al., 2004). The resulting data are consistent with an overall reaction mechanism proceeding from folded tetramers to dimeric species to unfolded apo-α and apo-β monomers. Accordingly, tetrameric assemblies exhibit a very rapid decay (Fig. 7C), that is concomitant with an intensity rise of dimeric species (Fig. 7D). These dimers undergo a decay process on a somewhat slower time scale, matching the rise of unfolded monomers (Fig. 7E). When considered in the context of other recent studies on the unfolding kinetics of large protein complexes (Chen and Smith, 2000; Wilson et al., 2005), the hemoglobin data discussed here suggest that the occurrence of complex reaction mechanisms involving several short-lived intermediates is a common feature for the denaturation of large multiprotein complexes.

C. Studying Protein Conformational Dynamics by Hydrogen Exchange Methods

Many proteins are known to adopt partially folded conformations under mildly denaturing solvent conditions. Studies on these semi-denatured states are of great importance for understanding a wide range of biological processes such as folding, amyloid formation, signal transduction, ligand-binding, and protein transport across membranes. Recent work has shown that some proteins exhibit a significant degree of disorder, even under physiological conditions where they are biologically active (Dyson and Wright, 2002).

Partially folded proteins are structurally heterogeneous ensembles, undergoing conformational fluctuations on time scales ranging from sub-nanoseconds to seconds. Experimental techniques capable of probing the dynamic nature of these species are crucial for obtaining a better understanding of their biophysical properties. One important approach in this area is based the use of hydrogen-deuterium exchange (HDX) (Krishna et al., 2004; Busenlehner and Armstrong, 2005). HDX at sites that are sterically shielded from the solvent, and/or involved in stable hydrogen bonds, is mediated by structural fluctuations of the protein. The exchange kinetics observed upon exposure of a protein to a D_2O-containing solvent system are, therefore, related to the conformational dynamics of the polypeptide chain. Brief opening events mediating exchange may correspond to global or subglobal unfolding/refolding transitions, or to local fluctuations (Krishna et al., 2004). The exchange mechanism in a strongly D_2O-enriched solvent system is usually described by

$$X-H_{closed} \underset{k_{close}}{\overset{k_{open}}{\rightleftarrows}} X-H_{open} \xrightarrow[D_2O]{k_{ch}} X-D \qquad (7)$$

where k_{open} and k_{close} are the rate constants for the opening and closing, respectively, of a particular exchangeable site. The chemical exchange rate constant, k_{ch}, represents the kinetics that would be expected for a fully unprotected hydrogen. For amide hydrogens, the k_{ch} value of any individual site is strongly affected by pD, and by the nature of neighboring amino acid side chains. Reference data obtained from dipeptide model compounds are available that allow the estimation of amide k_{ch} for any set of solvent conditions (Bai et al., 1993). In the so-called EX2 limit, characterized by $k_{close} \gg k_{ch}$, the overall exchange rate constant, k_{ex}, is given by $k_{ex} = K_{open}k_{ch}$, where $K_{open} = (k_{open}/k_{close})$ is the equilibrium constant of the opening reaction. Under EX2 conditions, most sites have to visit the open conformation many times before exchange occurs. Conversely, if $k_{ch} \gg k_{close}$ (the so-called EX1 regime), complete labeling will occur with the first opening event, such that $k_{ex} = k_{open}$.

NMR spectroscopy has traditionally been the method of choice for analyzing proteins in HDX studies (Krishna et al., 2004). However, in recent years, the use of ESI-MS for this purpose has become increasingly popular (Engen and Smith, 2001; Kaltashov and Eyles, 2002a). Every individual exchange event increases the mass of the protein by one Da. In contrast to NMR, ESI-MS data are not averaged over all the protein molecules in the sample. Instead, co-existing species can be detected, and their HDX properties can be monitored individually. One particularly attractive feature of ESI-MS is the possibility to clearly distinguish EX1 from EX2 exchange events. In the former case, spectra recorded at different times exhibit peaks

corresponding to the fully labeled and the unlabeled protein, respectively. As time proceeds, the intensity ratio of these peaks changes, but not their individual mass values. In contrast, EX2 kinetics give rise to a single peak that gradually moves to higher mass as HDX proceeds (Miranker et al., 1996; Konermann and Simmons, 2003; Ferraro et al., 2004).

Many previous MS-based studies have analyzed the HDX pattern of partially labeled proteins using proteolytic digestion approaches (Smith et al., 1997; Engen and Smith, 2001). These experiments provide spatially resolved information, i.e., the degree of structural flexibility can be directly mapped to specific regions along the polypeptide backbone. However, these studies rely on the use of acid quenching, which normally causes the complete breakdown of all protein-protein and protein-ligand interactions. As a consequence, it is not possible to correlate the observed HDX characteristics with individual binding states of a protein in solution. This problem can be circumvented by employing on-line ESI-MS approaches, analogous to the time-resolved experiments described in the preceding sections. Spatial resolution in these on-line studies may be obtained by using top-down gas-phase fragmentation techniques (Kaltashov and Eyles, 2002b; Xiao and Kaltashov, 2005).

Native holo-myoglobin (hMb, 17.5 kDa) has eight α-helices that form a hydrophobic pocket into which a heme group is bound. Unfolding causes a disruption of the heme-protein interactions, thereby generating apo-myoglobin (aMb). In a recent HDX study, the conformational dynamics of myoglobin have been explored in the presence of a moderate concentration of acetonitrile (27% v/v) at pD 9.3 (Simmons et al., 2003). The value of k_{ch} at this pD is around 10^3 s^{-1}. The ESI mass spectrum of the protein recorded under these semi-denaturing conditions reveals the presence of hMb and aMb in various conformations and heme binding states (Fig. 8A). It is noted that this spectrum represents an equilibrium situation; it does not change over time. Nonetheless, it is clear that any equilibrium is dynamic, such that the protein species represented by the different types of ions will be continuously involved in interconversion processes.

This interconversion, along with the structural dynamics of the various conformational species, can be visualized by tracking the mass distributions of the corresponding ionic signals. As an example, aMb^{14+} represents a relatively expanded apo-protein conformation in solution (Fig. 8B-D). With increasing labeling time these ions shift to higher mass,

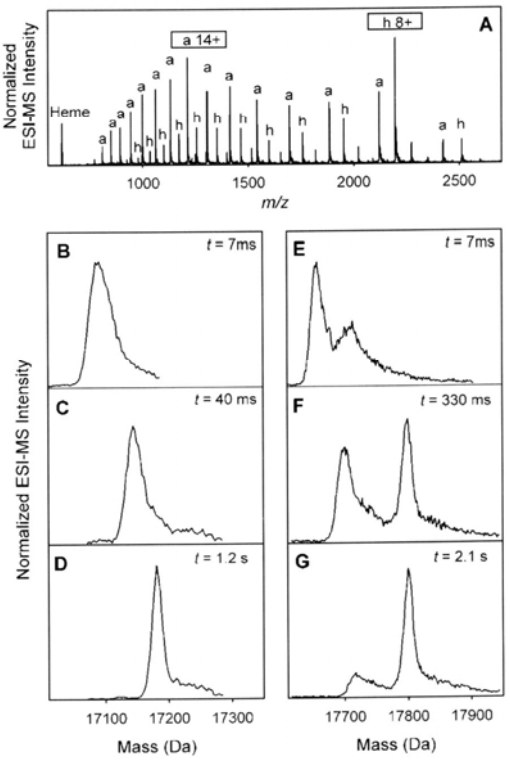

Fig. 8. Structural dynamics of myoglobin studied by time-resolved hydrogen-deuterium exchange (HDX) ESI-MS. (A) myoglobin spectrum recorded under semi-denaturing conditions (27% acetonitrile, pH 9.3). Notation: 'h' represents heme-bound holo-myoglobin (hMb), 'a' denotes heme-free apo-myoglobin (aMb). (B-D) mass distributions of the aMb^{14+} ionic species for selected time points. (E-G) mass distributions of the hMb^{8+} ionic species for selected time points. (Simmons et al., 2004, with permission).

indicating EX2 exchange, i.e., the occurrence of rapid unfolding/refolding events with closing rate constants $k_{cl} \gg 10^3$ s^{-1}. A more complex exchange behavior is exhibited by hMb^{8+} (Fig. 8E-G), which represents a native-like conformation of the holo-protein. For labeling times up to roughly 2 s, these protein ions show bimodal mass distributions. The relative intensity of the low mass peak decreases, and that of the high mass peak increases (EX1 behavior). This phenomenon indicates the occurrence of a slow aMb/hMb interconversion process in solution. In addition, a gradual shift to higher mass is observed for both peaks, which shows that the proteins also undergo more rapid structural fluctuations (EX2

exchange) (Simmons et al., 2003).

Another interesting approach is the use of double-mixing sequences, e.g., for combining time-resolved ESI-MS studies of the type discussed in III.A with on-line pulsed HDX. Experiments of this kind can provide even more information on protein conformational changes during folding. This is due to the fact that the HDX pattern and the ESI charge state distribution represent non-redundant probes of protein structure in solution. The charge state distribution reflects the overall compactness of the protein, whereas pulsed HDX reports on the intactness of the overall hydrogen bonding network, and on the solvent accessibility of exchangeable sites. The complementary nature of the two probes allows the detection of short-lived intermediates in cases where a cursory analysis indicates two-state behavior (Pan et al., 2005). A detailed discussion of these pulse-labeling approaches is beyond the scope of this chapter. Interested readers should consult the recent review of Konermann and Simmons (2003).

IV. Conclusions

In this chapter we described how time resolved mass spectrometry can be applied to biophysical questions like enzyme mechanisms and the dynamics and intermediates of protein (un)folding. Some specific examples are given to illustrate the range of different strategies that have been employed in this rapidly growing field. The key advantages of MS over many spectroscopic techniques are certainly the isotope specificity, the large time span that can be analyzed in on-line experiments and the enormous variety of different analytes that can be studied at physiological temperatures in solution. In this way, unique information can be gathered that, together with complementary spectroscopic data, is crucial for developing a comprehensive understanding of biophysical and biochemical reaction mechanisms.

Acknowledgments

LK thanks his students and post-docs that were involved in the work summarized in this chapter, in particular Douglas A. Simmons, Derek J. Wilson, and Jingxi Pan. Financial support for LK's laboratory was provided by the Natural Sciences and Engineering Research Council of Canada (NSERC), the Canada Foundation for Innovation (CFI), the Provincial Government of Ontario, The University of Western Ontario, and by the Canada Research Chairs Program. JM thanks his PhD student K. Beckmann for critically reading the manuscript and her contributions to the described research. He acknowledges support from the Deutsche Forschungsgemeinschaft (DFG; Me 1629/2-3) and the Max-Planck-Gesellschaft (MPG). WH acknowledges informative discussions with George Hoch, Murray Badger, Richard Radmer and support from the Human Frontiers Science Program Organization (RGP0029/2002).

References

An SM, Gardner WS and Kana T (2001) Simultaneous measurement of denitrification and nitrogen fixation using isotope pairing with membrane inlet mass spectrometry analysis. Appl Environ Microb 67: 1171–1178

Anfinsen CB (1973) Principles that govern the folding of protein chains. Science 181: 223–230

Bachmann A and Kiefhaber T (2001) Apparent two-state tendamistat folding is a sequential process along a defined route. J Mol Biol 306: 375–386

Bader KP and Roben A (1995) Mass spectrometric detection and analysis of nitrogen fixation in *Oscillatoria chalybea*. Z Naturforsch C 50: 199–204

Bader KP, Thibault P and Schmid GH (1983) A study on oxygen evolution and on the S-state distribution in thylakoid preparations of the filamentous blue-green alga *Oscillatoria chalybea*. Z Naturforsch C 38: 778–792

Bader KP, Thibault P and Schmid GH (1987) Study on the properties of the S3 state by mass spectrometry in the filamentous cyanobacterium *Oscillatoria chalybea*. Biochim Biophys Acta 893: 564–571

Bader KP, Renger G and Schmid GH (1993) A mass spectrometric analysis of the water splitting reaction. Photosynth Res 38: 355–361

Badger MR and Andrews TJ (1982) Photosynthesis and inorganic carbon usage by the marine cyanobacterium *Synechococcus* Sp. Plant Physiol 70: 517–523

Badger MR and Price GD (1989) Carbonic anhydrase activity associated with the cyanobacterium *Synechococcus* PCC7942. Plant Physiol 89: 51–60

Badger MR and Price GD (1994) The role of carbonic anhydrase in photosynthesis. Annu Rev Plant Phys 45: 369–392

Badger MR, Palmqvist K and Yu JW (1994) Measurement of CO_2 and HCO_3^- fluxes in cyanobacteria and microalgae during steady state photosynthesis. Physiol Plantarum 90: 529–536

Bai Y, Milne JS, Mayne L and Englander SW (1993) Primary structure effects on peptide group hydrogen exchange. Proteins: Struct Funct Genet 17: 75–86

Baltruschat H (2004) Differential electrochemical mass spectrometry. J Am Soc Mass Spectr 15: 1693–1706

Baltruschat H and Schmiemann U (1993) The adsorption of unsaturated organic species at single crystal electrodes studied by differential electrochemical mass spectrometry. Ber Bunsen

Phys Chem 97: 452–460
Beckmann M and Lloyd D (2001) Mass spectrometric monitoring of gases (CO_2, CH_4, O_2) in a mesotrophic peat core from Koparas Mire, Sweden. Global Change Biol 7: 171–180
Beckmann M, Sheppard SK and Lloyd D (2004) Mass spectrometric monitoring of gas dynamics in peat monoliths: Effects of temperature and diurnal cycles on emissions. Atmos Environ 38: 6907–6913
Beechem JM, Ameloot M and Brand L (1985) Global and target analysis of complex decay phenomena. Anal Instrum 14: 379–402
Berberan-Santos MN and Martinho JMG (1990) The integration of kinetic rate equations by matrix methods. J Chem Ed 67: 375–379
Bethke PC, Badger MR and Jones RL (2004) Apoplastic synthesis of nitric oxide by plant tissues. Plant Cell 16: 332–341
Britt RD, Campbell KA, Peloquin JM, Gilchrist ML, Aznar CP, Dicus MM, Robblee J and Messinger J (2004) Recent pulsed EPR studies of the Photosystem II oxygen evolving complex: Implications as to water oxidation mechanisms. Biochim Biophys Acta 1655: 158–171
Bruckenstein S and Gadde RR (1971) Use of a porous electrode for in situ mass spectrometric determination of volatile electrode reaction products. J Am Chem Soc 93: 793–794
Bruins AP, Covey TR and Henion JD (1987) Ion spray interface for combined liquid chromatography/atmospheric pressure ionization mass spectrometry. Anal Chem 59: 2642–2646
Brutscher B, Brüschweiler R and Ernst RR (1997) Backbone dynamics and structural characterization of the partially folded A state of ubiquitin by ^{1}H, ^{13}C and ^{15}N nuclear magnetic resonance spectroscopy. Biochemistry 36: 13043–13053
Busenlehner LS and Armstrong RN (2005) Insights into enzyme structure and dynamics elucidated by amide H/D exchange mass spectrometry. Arch Biochem Biophys 433: 34–46
Calvo KC, Weisenberger CR, Anderson LB and Klapper MH (1981) Permeable membrane mass spectrometric measurement of reaction kinetics. Anal Chem 53: 981–985
Canvin DT, Berry JA, Badger MR, Fock H and Osmond CB (1980) Oxygen exchange in leaves in the light. Plant Physiol 66: 302–307
Cartaxana P and Lloyd D (1999) N_2, N_2O and O_2 profiles in a Tagus estuary salt marsh. Estuar Coast Shelf S 48: 751–756
Chemical Rubber Company (2005) CRC Handbook of Chemistry and Physics. Chemical Rubber, Cleveland
Chen J and Smith DL (2000) Unfolding and disassembly of the chaperonin GroEL occurs via a tetradecameric intermediate with a folded equatorial domain. Biochemistry 39: 4250–4258
Chernushevich IV, Loboda AV and Thomson BA (2001) An introduction to quadrupole time-of-flight mass spectrometry. J Mass Spectrom 36: 849–865
Chowdhury SK, Katta V and Chait BT (1990) Probing conformational changes in proteins by mass spectrometry. J Am Chem Soc 112: 9012–9013
Christianson DW and Fierke CA (1996) Carbonic anhydrase: Evolution of the zinc binding site by nature and by design. Acc Chem Res 29: 331–339
Clausen J, Beckmann K, Junge W and Messinger J (2005) Evidence that bicarbonate is not the substrate in photosynthetic oxygen evolution. Plant Physiol 139: 1444–1450
Conrath U, Amoroso G, Kohle H and Sultemeyer DF (2004) Non-invasive online detection of nitric oxide from plants and some other organisms by mass spectrometry. Plant J 38: 1015–1022
Cournac L, Redding K, Ravenel J, Rumeau D, Josse EM, Kuntz M and Peltier G (2000) Electron flow between Photosystem II and oxygen in chloroplasts of Photosystem I deficient algae is mediated by a quinol oxidase involved in chlororespiration. J Biol Chem 275: 17256–17262
Demmers JAA, Haverkamp J, Heck AJR, Koeppe RE and Killian A (2000) Electrospray ionization mass spectrometry as a tool to analyze hydrogen/deuterium exchange kinetics of transmembrane peptides in lipid bilayers. Proc Natl Acad Sci USA 97: 3189–3194
Dobson CM (2003) Protein folding and misfolding. Nature 426: 884–890
Douglas DJ, Frank AJ and Mao D (2005) Linear ion traps in mass spectrometry. Mass Spectrom Rev 24: 1–29
Duda DM, Tu CK, Fisher SZ, An HQ, Yoshioka C, Govindasamy L, Laipis PJ, Agbandje-McKenna M, Silverman DN and McKenna R (2005) Human carbonic anhydrase III: Structural and kinetic study of catalysis and proton transfer. Biochemistry 44: 10046–10053
Dyson HJ and Wright PE (2002) Coupling of folding and binding for unstructured proteins. Curr Op Struct Biol 12: 54–60
Engen JR and Smith DL (2001) Investigating protein structure and dynamics by hydrogen exchange mass spectrometry. Anal Chem 73: 256A–265A
Fenn JB (2003) Electrospray wings for molecular elephants (Nobel Lecture). Angew Chem Int Ed 42: 3871–3894
Fenn JB, Mann M, Meng CK, Wong SF and Whitehouse CM (1989) Electrospray ionization for mass spectrometry of large biomolecules. Science 246: 64–71
Ferraro DM, Lazo ND and Robertson AD (2004) EX1 hydrogen exchange and protein folding. Biochemistry 43: 587–594
Fisher Z, Prada JAH, Tu C, Duda D, Yoshioka C, An HQ, Govindasamy L, Silverman DN and McKenna R (2005) Structural and kinetic characterization of active site histidine as a proton shuttle in catalysis by human carbonic anhydrase II. Biochemistry 44: 1097–1105
Govindjee, Owens OV and Hock G (1963) A mass-spectroscopic study of the Emerson enhancement effect. Biochim Biophys Acta 75: 281–284
Griffith WP and Kaltashov IA (2003) Highly asymmetric interactions between globin chains during hemoglobin assembly revealed by electrospray ionization mass spectrometry. Biochemistry 42: 10024–10033
Gross JW and Frey PA (2002) Rapid mix-quench MALDI-TOF mass spectrometry for analysis of enzymatic systems. Meth Enzymol 354: 27–49
Hanson DT, Franklin LA, Samuelsson G and Badger MR (2003) The *Chlamydomonas reinhardtii* cia3 mutant lacking a thylakoid lumen-localized carbonic anhydrase is limited by CO_2 supply to rubisco and not Photosystem II function in vivo. Plant Physiol 132: 2267–2275
Hartung T and Baltruschat H (1990) Differential electrochemical mass spectrometry using smooth electrodes: Adsorption and H/D-exchange reactions of benzene on Pt. Langmuir 6: 953–957
Heck AJR and Van den Heuvel RHH (2004) Investigation of intact protein complexes by mass spectrometry. Mass Spectrom Rev 23: 368–389

Higuchi Y and Yagi T (1999) Liberation of hydrogen sulfide during the catalytic action of *Desulfovibrio* hydrogenase under the atmosphere of hydrogen. Biophys Res Comm 255: 295–299

Higuchi Y, Toujou F, Tsukamoto K and Yagi T (2000) The presence of a SO molecule in [NiFe] hydrogenase from *Desulfovibrio vulgaris Miyazaki* as detected by mass spectrometry. J Inorg Biochem 80: 205–211

Hillier W and Messinger J (2005) Mechanism of photosynthetic oxygen production. In: Wydrzynski T and Satoh K (eds) Photosystem II: The Water/Plastoquinone Oxidoreductase in Photosynthesis (Advances in Photosynthesis and Respiration, Vol 22) pp 567–608. Springer, Dordrecht

Hillier W and Wydrzynski T (2004) Substrate water interactions within the Photosystem II oxygen evolving complex. Phys Chem Chem Phys 6: 4882–4889

Hillier W, Messinger J and Wydrzynski T (1998) Kinetic determination of the fast exchanging substrate water molecule in the S_3 state of Photosystem II. Biochemistry 37: 16908–16914

Hillier W, McConnell I, Badger MR, Boussac A, Klimov VV, Dismukes GC and Wydrzynski T (2006) Quantitative assessment of intrinsic carbonic anhydrase activity and the capacity for bicarbonate oxidation in Photosystem II. Biochemistry 5: 2094–102

Hoch G and Kok B (1963) A mass spectrometer inlet system for sampling gases dissolved in liquid phases. Arch Biochem Biophys 101: 160–170

Hoch G, Owens OHV and Kok B (1963) Photosynthesis and Respiration. Arch Biochem Biophys 101: 171–180

Holzwarth AR (1995) Time-resolved fluorescence spectroscopy. Meth Enzymol 246: 334–362

Houston CT, Taylor WP, Widlanski TS and Reilly JP (2000) Investigation of enzyme kinetics using quench-flow techniques with MALDI TOF mass spectrometry. Anal Chem 72: 3311–3319

Johnson RC, Cooks RG, Allen TM, Cisper ME and Hemberger PH (2000) Membrane introduction mass spectrometry: Trends and applications. Mass Spectrom Rev 19: 1–37

Kaltashov IA and Eyles SJ (2002a) Crossing the phase boundary to study protein dynamics and function: Combination of amide hydrogen exchange in solution and ion fragmentation in the gas phase. J Mass Spectrom 37: 557–565

Kaltashov IA and Eyles SJ (2002b) Studies of biomolecular conformations and conformational dynamics by mass spectrometry. Mass Spectrom Rev 21: 37–71

Kaltashov IA and Eyles SJ (2005) Mass spectrometry in biophysics. John Wiley and Sons, Hoboken

Karas M and Hillenkamp F (1988) Laser desorption ionization of proteins with molecular masses exceeding 10,000 Daltons. Anal Chem 60: 2299–2301

Kebarle P and Ho Y (1997) On the mechanism of electrospray mass spectrometry. In: Cole RB (ed) Electrospray Ionization Mass Spectrometry, pp 3–63. John Wiley and Sons, New York

Knight JB, Vishwanath A, Brody JP and Austin RH (1998) Hydrodynamic focusing on a silicon chip: Mixing nanoliters in microseconds. Phys Rev Lett 80: 3863–3866

Kok B and Varner JE (1967) Extraterrestial life detection based on oxygen isotope exchange reactions. Science 155: 1110–1112

Kolakowski BM and Konermann L (2001) From small-molecule reactions to protein folding: Studying biochemical kinetics by stopped-flow electrospray mass spectrometry. Anal Biochem 292: 107–114

Konermann L (1999) Monitoring reaction kinetics by continuous-flow methods: The effects of convection and molecular diffusion under laminar flow conditions. J Phys Chem A 103: 7210–7216

Konermann L and Douglas DJ (2002) Pre-steady-state kinetics of enzymatic reactions studied by electrospray mass spectrometry with on-line rapid-mixing techniques. Meth Enzymol 354: 50–64

Konermann L and Simmons DA (2003) Protein-folding kinetics and mechanisms studied by pulse-labeling and mass spectrometry. Mass Spectrom Rev 22: 1–26

Konermann L, Collings BA and Douglas DJ (1997) Cytochrome *c* folding kinetics studied by time-resolved electrospray ionization mass spectrometry. Biochemistry 36: 5554–5559

Konermann L, Silva EA and Sogbein OF (2001) Electrochemically induced pH changes resulting in protein unfolding in the ion source of an electrospray mass spectrometer. Anal Chem 73: 4836–4844

Krasna AI (1978) Oxygen stable hydrogenase and assay. Meth Enzymol 53: 296–314

Kretschmann H and Witt HT (1993) Chemical reduction of the water splitting enzyme system of photosynthesis and its light induced reoxidation characterized by optical and mass spectrometric measurements: A basis for the estimation of the states of the redox active manganese and of water in the quaternary oxygen evolving S-state cycle. Biochim Biophys Acta 1144: 331–345

Krishna MMG, Hoang L, Lin Y and Englander SW (2004) Hydrogen exchange methods to study protein folding. Methods 34: 51–64

Laiko VV, Baldwin MA and Burlingame AL (2000) Atmospheric pressure matrix-assisted laser desorption/ionization mass spectrometry. Anal Chem 72: 652–657

Li Z, Sau AK, Shen S, Whitehouse C, Baasov T and Anderson KS (2003) A snapshot of enzyme catalysis using electrospray mass spectrometry. J Am Chem Soc 125: 9938–9939

Liesener A and Karst U (2005) Monitoring enzymatic conversions by mass spectrometry: A critical review. Anal Bioanal Chem 382: 1451–1464

Lindskog S and Coleman JE (1973) Catalytic mechanism of carbonic anhydrase. Proc Natl Acad Sci USA 70: 2505–2508

Lloyd D, Thomas KL, Cowie G, Tammam JD and Williams AG (2002) Direct interface of chemistry to microbiological systems: Membrane inlet mass spectrometry. J Microbiol Meth 48: 289–302

Mano J, Takahashi M-A and Asada K (1987) Oxygen evolution from hydrogen peroxide in Photosystem II: Flash induced catalytic activity of water oxidizing Photosystem II membranes. Biochemistry 26: 2495–2501

Mao FM and Leck JH (1987) The quadrupole mass spectrometer in practical operation. Vacuum 37: 669–675

Marshall AG, Hendrickson CL and Jackson GS (1998) Fourier transform ion cyclotron resonance mass spectrometry: A primer. Mass Spectrom Rev 17: 1–35

Martin JP, Johnson RD, Kok B and Radmer R (1975) Unified mars life detection system. J Astronaut Sci 23: 99–119

Maxwell K, Badger MR and Osmond CB (1998) A comparison of CO_2 and O_2 exchange patterns and the relationship with chlorophyll fluorescence during photosynthesis in C_3 and CAM plants. Aust J Plant Physiol 25: 45–52

McEvoy JP and Brudvig GW (2004) Structure based mechanism of photosynthetic water oxidation. Phys Chem Chem Phys 6: 4754–4763

Messinger J (2004) Evaluation of different mechanistic proposals

for water oxidation in photosynthesis on the basis of Mn_4O_xCa structures for the catalytic site and spectroscopic data. Phys Chem Chem Phys 6: 4764–4771

Messinger J, Badger M and Wydrzynski T (1995) Detection of one slowly exchanging substrate water molecule in the S_3 state of Photosystem II. Proc Natl Acad Sci USA 92: 3209–3213

Meyer S, Koch R and Metzger JO (2003) Investigation of reactive intermediates of chemical reactions in solution by electrospray ionization mass spectrometry: Radical cation chain reactions. Angew Chem Int Edit 42: 4700–4703

Miranker A, Robinson CV, Radford SE and Dobson CM (1996) Investigation of protein folding by mass spectrometry. FASEB J 10: 93–101

Norris AJ, Whitelegge JP, Faull KF and Toyokuni T (2001) Analysis of enzyme kinetics using electrospray ionization mass spectrometry and multiple reaction monitoring: Fucosyltransferase V. Biochemistry 40: 3774–3779

Northrop DB and Simpson FB (1997) Beyond enzyme kinetics: Direct determination of mechanisms by stopped-flow mass spectrometry. Bioorg Med Chem 5: 641–644

Pain RH (2000) Mechanisms of Protein Folding. Oxford University Press, New York

Pan JX, Wilson DJ and Konermann L (2005) Pulsed hydrogen exchange and electrospray charge-state distribution as complementary probes of protein structure in kinetic experiments: Implications for ubiquitin folding. Biochemistry 44: 8627–8633

Poulsen AK, Rompel A and McKenzie CJ (2005) Water oxidation catalyzed by a dinuclear Mn complex: A functional model for the oxygen-evolving center of Photosystem II. Angew Chem Int Edit 44: 6916–6920

Prior JJ, Christie PD, Murray RJ, Ormejohnson WH and Cooney CL (1995) Continuous monitoring of nitrogenase activity in *Azotobacter vinelandii* fermentation using off-gas mass spectrometry. Biotechnol Bioeng 47: 373–383

Radmer R (1979) Mass spectrometric determination of hydroxylamine photo-oxidation by illuminated chloroplasts. Biochim Biophys Acta 546: 418–425

Radmer R and Kok B (1971) Unified procedure for detection of life on mars. Science 174: 233–239

Radmer R and Ollinger O (1980a) Measurement of the oxygen cycle: The mass spectrometric analysis of gases dissolved in a liquid phase. Meth Enzymol 69: 547–560

Radmer R and Ollinger O (1980b) Light driven uptake of oxygen, carbon dioxide, and bicarbonate by the green algae *Scenedesmus*. Plant Physiol 65: 723–729

Radmer R and Ollinger O (1980c) Isotopic composition of photosynthetic O_2 flash yields in the presence of $H_2{}^{18}O$ and $HC^{18}O_3^-$. FEBS Lett 110: 57–61

Radmer R and Ollinger O (1981) Mass spectrometric studies of hydrazine photooxidation by illuminated chloroplasts. Biochim Biophys Acta 637: 80–87

Radmer R and Ollinger O (1982) Nitrogen and oxygen evolution by hydroxylamine treated chloroplasts. FEBS Lett 144: 162–166

Radmer R and Ollinger O (1983) Topography of the O_2 evolving site determined with water analogs. FEBS Lett 152: 39–43

Radmer R and Ollinger O (1986) Do the higher oxidation states of the photosynthetic O_2 evolving system contain bound H_2O. FEBS Lett 195: 285–289

Radmer RJ, Kok B and Martin JP (1976) System for biological and soil chemical tests on a planetary lander. J Spacecraft Rockets 13: 719–726

Renger G (2001) Photosynthetic water oxidation to molecular oxygen: Apparatus and mechanism. Biochim Biophys Acta 1503: 210–228

Ribas-Carbo M, Robinson SA and Giles L (2005) The application of oxygen isotope technique to respiratory pathway partitioning. In: Lambers H and Ribas-Carbo M (eds) Plant Respiration: From Cell to Ecosystem (Advances in Photosynthesis and Respiration, Vol 18), pp 31–42. Springer, Dordrecht

Roboz J (1968) Mass spectrometry: Instrumentation and techniques. Wiley, New York

Ruuska SA, Badger MR, Andrews TJ and von Caemmerer S (2000) Photosynthetic electron sinks in transgenic tobacco with reduced amounts of Rubisco: Little evidence for significant Mehler reaction. J Exp Bot 51: 357–368

Schermann SM, Simmons DA and Konermann L (2005) Mass spectrometry-based approaches to protein-ligand interactions. Exp Rev Proteomics 2: 475–485

Shastry MCR, Luck SD and Roder H (1998) A continuous-flow mixing method to monitor reactions on the microsecond time scale. Biophys J 74: 2714–2721

Shima S, Lyon EJ, Thauer RK, Mienert B and Bill E (2005) Mössbauer studies of the iron-sulfur cluster-free hydrogenase: The electronic state of the mononuclear Fe active site. J Am Chem Soc 127: 10430–10435

Shoemaker BA, Portman JJ and Wolynes PG (2000) Speeding molecular recognition by using the folding funnel: The fly-casting mechanism. Proc Natl Acad Sci USA 97: 8868–8873

Silva ACB, Augusti R, Dalmazio I, Windmoller D and Lago RM (1999) MIMS evaluation of pervaporation processes. Phys Chem Chem Phys 1: 2501–2504

Silverman DN (1982) Carbonic anhydrase ^{18}O exchange catalyzed by an enzyme with rate contributing proton transfer steps. Methods in Enzymology 87: 732–752

Silverman DN and Tu CK (1976) Carbonic anhydrase catalyzed hydration studied by ^{13}C and ^{18}O labeling of carbon dioxide. J Am Chem Soc 98: 978–984

Simmons DA, Dunn SD and Konermann L (2003) Conformational dynamics of partially denatured myoglobin studied by time-resolved electrospray mass spectrometry with online hydrogen-deuterium exchange. Biochemistry 42: 9248–9248

Simmons DA, Wilson DJ, Lajoie GA, Doherty-Kirby A and Konermann L (2004) Subunit disassembly and unfolding kinetics of hemoglobin studied by time-resolved electrospray mass spectrometry. Biochemistry 43: 14792–14801

Siuzdak G (1996) Mass spectrometry for biotechnology. Academic Press, New York

Smith DL, Deng Y and Zhang Z (1997) Probing the noncovalent structure of proteins by amide hydrogen exchange mass spectrometry. J Mass Spectrom 32: 135–146

So AKC, Van Spall HGC, Coleman JR and Espie GS (1998) Catalytic exchange of ^{18}O from $^{13}C^{18}O$-labelled CO_2 by wild-type cells and *ecaA, ecaB,* and ccaA mutants of the cyanobacteria *Synechococcus* PCC7942 and *Synechocystis* PCC6803. Can J Bot 76: 1153–1160

Tanaka K (2003) The origin of macromolecule ionization by laser irradiation (Nobel Lecture). Angew Chem Int Edit 42: 3861–3870

Tegtmeyer D, Heindrichs A and Heitbaum J (1989) Electrochemical on line mass spectrometry on a rotating electrode

inlet system. Ber Bunsen Phys Chem 93: 201–206
Tortell PD (2005) Dissolved gas measurements in oceanic waters made by membrane inlet mass spectrometry. Limnol Oceanogr Meth 3: 24–37
Vignais PM (2005) H/D exchange reactions and mechanistic aspects of the hydrogenases. Coordin Chem Rev 249: 1677–1690
Whitelegge JP, Le Coutre J, Lee JC, Engel CK, Prive GG, Faull KF and Kaback HR (1999) Toward the bilayer proteome, electrospray ionization-mass spectrometry of large, intact transmembrane proteins. Proc Natl Acad Sci USA 96: 10695–10698
Wilson DJ and Konermann L (2003) A capillary mixer with adjustable reaction chamber volume for millisecond time-resolved studies by electrospray mass spectrometry. Anal Chem 75: 6408–6414
Wilson DJ and Konermann L (2004) Mechanistic studies on enzymatic reactions by electrospray ionization MS using a capillary mixer with adjustable reaction chamber volume for time resolved measurements. Anal Chem 76: 2537–2543
Wilson DJ and Konermann L (2005) Ultrarapid desalting of protein solutions for electrospray mass spectrometry in a microchannel laminar flow device. Anal Chem 77: 6887–6894
Wilson DJ, Rafferty SP and Konermann L (2005) Kinetic unfolding mechanism of the inducible nitric oxide synthase oxygenase domain determined by time-resolved electrospray mass spectrometry. Biochemistry 44: 2276–2283
Wittung-Stafshede P (2002) Role of cofactors in protein folding. Acc Chem Res 35: 201–208
Wolter O and Heitbaum J (1984) Differential electrochemical mass spectroscopy (DEMS) — a new method for the study of electrode processes. Ber Bunsen Phys Chem 88: 2–6
Xiao H and Kaltashov IA (2005) Transient structural disorder as a facilitator of protein ligand binding: Native H/D exchange-mass spectrometry study of cellular retinoic acid binding protein I. J Am Soc Mass Spectrom 16: 869–879
Yano J, Kern J, Sauer K, Latimer MJ, Pushkar Y, Biesiadka J, Loll B, Saenger W, Messinger J, Zouni A and Yachandra VK (2006) Where water is oxidized to dioxygene: Structure of the photosynthetic Mn_4Ca cluster. Science 314: 821–825
Zechel DL, Konermann L, Withers SG and Douglas DJ (1998) Pre-steady state kinetic analysis of an enzymatic reaction monitored by time-resolved electrospray ionization mass spectrometry. Biochemistry 37: 7664–7669